Short-Range Ultraviolet Communication System using NOMA

A Thesis Submitted to the Department of Computer Science and Communication Engineering, the Graduate School of Fundamental Science and Engineering of Waseda University in Partial Fulfilment of the Requirements for the Degree of Master of Engineering.

Submission Date: July 18, 2022

Tokyo, Japan

AJGAONKAR, SWARALI ASHISH

(5120FG01-8)

Advisor: Prof. Shimamoto Shigeru

Research Guidance: Research on Wireless Network Systems

Table of Content

List of Figures:

List of Table

List of Equation

Acknowledgement

I want to express my gratitude to Prof. Shimamoto Shigeru for giving me the opportunity to do research and providing invaluable guidance throughout this research for his two years of advice, assistance, encouragement, and patience. It is an enormous honour for me to have him as my advisor and to get to study and work for two years in Shimamoto Lab. Professor Shimamoto Shigeru discussed the study direction with me when I discovered my interest in wireless optical communication more specifically in ultraviolet communication area and always provided me with valuable advice regarding my research problems. He always provided me with solutions to my research problems whenever I stumbled upon them.

And I want to thank Prof. Jiang Liu, the assistant professor of our lab. She offered me a lot of advice and motivated me whenever I come across research-related issues. I'm really grateful for the group member Tachikawa Wataru's assistance. Successfully I could able to completed my experiment with his help.

Additionally, I'm grateful to Wang Huan and Dhakal Dhruba, my seniors. Despite the fact that we are not in the same group, we frequently discussed my research-related challenges and both offered encouragement.

Finally, I'd want to express my gratitude to my family, particularly my parents and grandparents, who have given me their support and enabled me to pursue a master's degree at Waseda University. Finally, my thanks go to all the people who have supported me to complete the research work directly or indirectly.

Abstract

A type of wireless communication known as optical wireless communication (OWC) uses light waves to transmit signals. Unguided visible, IR, or UV light are all examples of these light waves. Usually, short-range communication systems make use of it. If the Line of Sight (LOS) link is obstructed or otherwise compromised, VLC and IR are not applicable. Significant scattering occurs with UV photons. In order to set up a communication link with a direct Line of Sight (LOS) path or with no other practical alternative, they give UV communications an excessive degree of planning latitude. The Binary Phase Shift Keying modulation technique, which uses Visible Light Communication as a medium of communication without taking distance into consideration, has been employed in previous research.

Ultraviolet (band A) light has been used as a communication medium in this research. This area is referred to as a solar-blind area because the ozone layer mainly blocks solar light in the UV-band-C spectrum. As a result, there is relatively low background noise. UV-band-A has smaller propagation losses than UV-band-C even while ambient light noise is present. With high output power density and high security, UV-A LEDs can operate at high currents of up to 800mA. Line of Sight (LOS) communication and a very low data rate are drawbacks of infrared light.

The NOMA-OFDM techniques provide the framework of the proposed schemes. The primary processes used in this system are Signal Interference Cancellation (SIC), Non-Orthogonal Multiple Access (NOMA) superposition, and Orthogonal Frequency Division Multiplexing (OFDM) Modulation. Each user in NOMA operates simultaneously in the same band, and it is possible to distinguish one user from another by their power output. NOMA uses superposition coding at the transmitter to enable the successive interference cancellation (SIC) receiver to distinguish between users in both the uplink and the downlink channels. For users 1 and 2, we have considered the NOMA strategy. Orthogonal Frequency Division Multiplexing (OFDM),

a digital multi-carrier modulation technology, extends the concept of single subcarrier modulation by using multiple subcarriers within a single channel. Instead of using a single subcarrier to transmit a high-rate stream of data, OFDM uses a large number of closely spaced, orthogonal subcarriers that are transmitted in sequence.

The experiment uses MATLAB software, GNU Radio, and LimeSDR hardware. As it demonstrates, all signal processing, including mapping, IFFT, and other techniques, will initially be carried out in MATLAB. Utilizing LimeSDR, Power Amplifier (PA), Bias Tee, LED, and APD detector, the real hardware experiment is carried out. Using the UV-A LED and the Quadrature Phase Shift Keying (QPSK) and Orthogonal Frequency Division Multiplexing (OFDM) modulation schemes, respectively, a bit error ratio (BER) of 4.30×10^{-4} is achieved at a distance of 1.5 m using Quadrature Phase Shift Keying (QPSK) and Orthogonal Frequency Division Multiplexing (OFDM) modulation schemes, respectively. Additionally, we compared the Bit Error Ratio (BER) for the modulation schemes PSK, 4-QAM, and QPSK. The BER graph demonstrates that, among all transmission modulation types, QPSK modulation performed best across all SNR levels; particularly, at 10 dB, we obtained 10^{-4} whereas QAM and PSK modulation are at 10^{-2} and 10^{-1} respectively. Only the 2-user case was taken into consideration, however future research may expand to the 4-user or 8-user (n-user) scenarios.

Chapter 1
Introduction

1.1 Background:

Because it has a large unlicensed bandwidth, no RF interference, is very secure, has cheap device costs, weights, and lengths, and can support high data speeds due to this large bandwidth, optical wireless communication (OWC) is seen as having a larger potential for RF communication[1]. Visible light communication (VLC), infrared communication (IR), and ultraviolet communication (UV) are the three main categories under which OWC can be categorized. The region of the electromagnetic spectrum that is visible to the human eye is known as the visible spectrum. The wavelength range is between 380 and 750 nanometers. On the other hand, infrared light is invisible to the human sight. With a wavelength ranging from 100 nm to 400 nm, ultraviolet light is also an electromagnetic radiation. VLC and IR are not applicable if the Line of Sight (LOS) link is blocked or otherwise hindered. UV rays have significant scattering properties. They provide UV communications an excessive amount of flexibility for planning a communication link with a direct Line of Sight (LOS) path or no other viable alternate way [2]. It can be applied in many different situations, including short-range data communications, airplane landing in foggy conditions, missile route detection, underwater communications, and many more [9].

Three sub-bands compose the UV wavelength band: UV-band-A (320 to 420 nm), UV-band-B (290 to 320 nm), and UV-band-C (100 to 290 nm). Every sub-band has unique characteristics that may limit or broaden its applications. Since the ozone layer primarily blocks solar light in UV-band-C, this region is known as a solar-blind area. As a result, the background noise level is quite low [3]. While there are noises from ambient lights, UV-band-A has lower propagation losses than UV-band-C [4].

As a modulation scheme, we consider Orthogonal Frequency Division Multiplexing (OFDM), and as a multiple access scheme, we consider NOMA. It is widely used in predictable 4G networks, in which facts for each consumer are assigned to a subset of sub-carriers. In NOMA, on the other hand, all subcarriers may be used by any consumer. Figure 1 illustrates OFDM and NOMA spectrum sharing for two users. The concept is applicable to both uplink and downlink transmission [8].

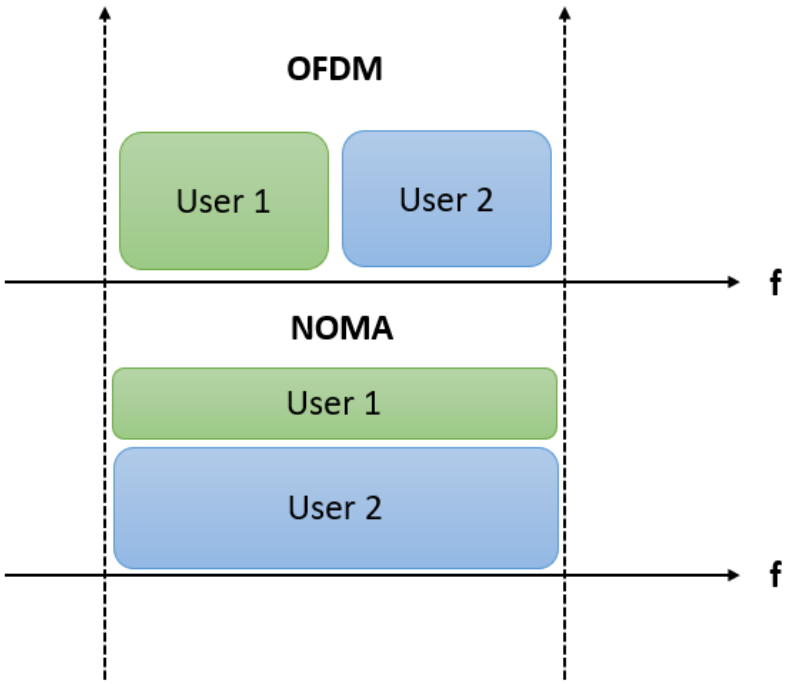

Figure 1: Spectrum sharing for OFDM and NOMA for two users

As a result, we have considered developing a UV-band-A short-range communication system using NOMA-OFDM techniques. The NOMA scheme provides users with orthogonal access in time, frequency, code, or space. Numerous users can use the same frequency bandwidth in NOMA, and they are distinguished by the power values that are assigned to them. The frequency resources can be used more effectively when NOMA and OFDM are deployed concurrently. The advantages of using the NOMA-OFDM approach in a system are that it maximizes bandwidth, increases computational complexity, and reduces decoding delay at the receiver.

A promising downlink Multiple Access scheme that achieves high spectral efficiency by combining superposition coding on the transmitter and successive interference cancellation (SIC) on the receiver [5]. When the signal is received by the system, we must use MATLAB to method and demodulate it. Using the successive interference cancellation (SIC) method, we can distinguish these different signals and calculate the overall performance of the NOMA-OFDM system in terms of Bit Error Ratio (BER). NOMA-OFDM strengthens the signal.

1.2 Related Work

Ultraviolet (UV) communications are currently gaining popularity due to some advantages over visible light communications. Because of the high background noise, solar radiation has a strong influence on visible-light-based optical communication links [8]. UV communication systems are investigated in a variety of environments, including indoor and outdoor scenarios, short-range data communications, and long-distance NLOS communication links. The reported studies are almost all focusing on UV in the solar-blind region because it has reduced environmental noises and UV devices were previously mostly manufactured for this region. There is currently a trend of research in UV-band-A due to its much lower propagation losses and the availability of devices in this band for commercial use [3].

Because of advantages such as low solar background noise and the ability to organize communication in the absence of direct visibility, invisible ultraviolet LEDs and the technology for detecting ultraviolet rays have gradually become an important topic of study in recent years (NLOS). [8]. The low modulation bandwidth of deep-ultraviolet (UV) light sources is considered to be the primary reason for deep-UV communications data transmission rate limitations. Previous research has demonstrated high-bandwidth III-nitride micro light-emitting diodes (LED) emitting in

the UV-C region, as well as their applications in deep-UV communication systems. Using the UV-C LED, data transmission rates of up to 800 Mbps and 1.1 Gbps are achieved with a bit error ratio of 3.8 × 10−4 respectively, assuming on-off keying and orthogonal frequency-division multiplexing modulation schemes [9].

In [10], a solar-blind region 265-nm LED array is used for light source under on-off keying (OOK)/PPM modulation with a channel length of 100 m, and its potential for subsea FSO is investigated. This system's data rate is listed as 2.4 kbps. An experimental study was conducted in [11] using a single input single output (SISO) and then a multiple input multiple output (2x2 MIMO) scheme for a solar-blind UV 265 nm LED array as a light source under intensity modulation direct detection (IM/DD), with a channel length of 30 m. An experimental investigation using UV-band-B near a solar-blind region with 294-nm LED as the light source for this communication link was previously noted. For a diffuse LOS link and a very short distance of 8 cm, the signal is modulated by quadrature amplitude modulation (QAM) with orthogonal frequency division multiplexing (OFDM), and the data rate of this system is reported as 71 Mbps using 8-QAM-OFDM [12].

Chapter 2

Ultraviolet Communication

2.1 Ultraviolet Light Sources

2.1.1 Ultraviolet Light

UV radiation is defined as having a wavelength ranging from 100 nm to 400 nm in the electromagnetic spectrum. These wavelengths are shorter than visible light wavelengths and longer than X-ray wavelengths. UV light is classified into three types: UVA (wavelengths between 315 and 400 nm), UVB (wavelengths between 280 and 315 nm), and UVC (wavelengths between 100 and 280 nm).

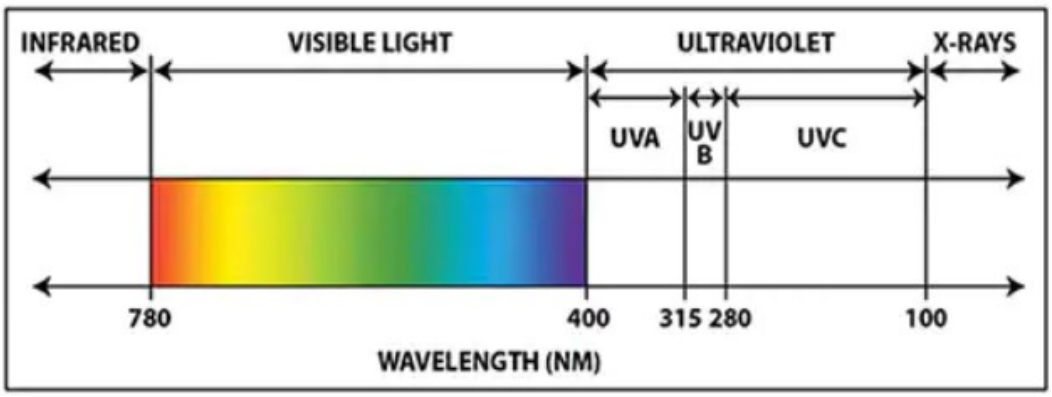

Figure 2: UV Wavelengths [13]

The sun emits ultraviolet radiation with wavelengths ranging from 100 to 400 nm. At the edge of the Earth's atmosphere, sunlight is composed of approximately 50% infrared (IR), 40% visible, and 10% ultraviolet light. When sunlight reaches the Earth's surface at its highest point, it is composed of 53 % infrared, 44 % visible, and % ultraviolet. Approximately 95 % of the UV that reaches the ground is Ultraviolet A and

% is Ultraviolet B. The upper atmosphere absorbs a large portion of the UVC wavelengths, which produces ozone in the ozone layer. The ozone layer absorbs the majority of UVB and the remainder of UVC that is not already absorbed by oxygen [13].

2.1.2 The UV Spectrum:

I. **UV-A:** This is the wavelength range from 400 to 315 nm. The ozone layer does not absorb UVA. UV-A light has the longest wavelength and is, therefore, the least dangerous. It is more commonly known as "black light," and many artists and celebrators use its ability to cause objects to emit fluorescence (a colored glowing effect) in their designs [14].

II. **UV- B:** This is the wavelength range from 315 to 280 nm. The ozone layer absorbs the majority of the Sun's UVB energy, but some escapes. With prolonged exposure, this causes sunburns as well as an increase in the risk of skin cancer and other cellular damage. The ozone in the Earth's atmosphere absorbs approximately 95% of all UV-B light [14].

III. **UV- C:** This is the wavelength range from 280 nm to 100 nm. Because of its high energy, UV light in this range is used in sterilization procedures. UV-C is extremely dangerous because it is completely absorbed by the ozone layer and upper atmosphere. It is frequently used as a disinfectant in food, air, and water to kill microorganisms by destroying the nucleic acids in their cells [14].

IV. **Extreme Ultraviolet (EUV) Light:** This is the wavelength range of 10-100nm. It can only travel in a vacuum and is completely absorbed by the Earth's atmosphere. The ionosphere is formed when EUV radiation ionizes the upper atmosphere. Furthermore, EUV waves from the Sun heat the Earth's

thermosphere. Because solar EUV waves cannot penetrate the atmosphere, scientists must use rockets and satellites to measure them. [14]

2.1.3 Uses of Ultraviolet light and its Effects [15][16]:

i. UVB exposure stimulates the production of vitamin D, which our bodies require. Because window glass absorbs UVB, people must go outside to take advantage
ii. The ability of UV to inactivate bacteria and viruses is extended by using UVC produced artificially to sterilise surfaces such as medical equipment. They're also used in water treatment facilities.
iii. Because most UV light is blocked by the atmosphere, space-based telescopes such as the Hubble Space Telescope are used to observe the universe in ultraviolet light. A complex process that uses UVC light to kill bacteria in the air.
iv. UV light is used to cure and form bonds in several adhesives. This method is used by some 3D printers to cure the resin used in the printing process.
v. Fluorescent dye that allows the ink to reflect vividly in sunlight and glow brightly in the dark when exposed to a UV lamp. UV and fluorescence can be used to create efficient lighting for offices, workshops, and our own homes.

Effects of UV Light [15]:

i. Depletion of the ozone layer reduces our atmosphere's natural protection from the sun's harmful ultraviolet (UV) radiation.
ii. Excessive UV exposure can harm your eye's dioptric system and retina, which is why staring at the sun, even during a solar eclipse, is a bad idea.
iii. This is the most well-known effect of UV light, as UVB and UVA exposure will result in a suntan or sunburn. Skin cancer is a more lethal side effect of UV light.

2.1.4 UV LED

- UV LEDs emit visible light because their output ranges from the violet to the ultraviolet range of the spectrum.
- UV LEDs are available in a wide range of spectral wavelengths ranging from 265 nm to 400 nm. This enables the purchase of UV LEDs to generate UVA, UVB, or UVC light and allows LEDs to be used in designs that would previously require more power-hungry traditional solutions [15].
- LEDs are increasingly being used in places where UV lamps (mercury, xenon, amalgam, excimer) have been used for decades.
- UV-LED flux density, stability, and life hours improvements have made UV LEDs a viable replacement for traditional UV light sources such as mercury arc lamps, arch lamps, hot and cold cathode lamps, and grid lamps.
- UV LEDs are more environmentally friendly because they contain no harmful mercury, produce no ozone, and use less energy [20].
- The following are some of the most common LED applications:
    - Air Purification
    - Surface Sterilization
    - Water Disinfection
    - Hospital Sanitization
    - Germicidal purification

Figure 3: Germicidal UV Light(7gadgets.com)

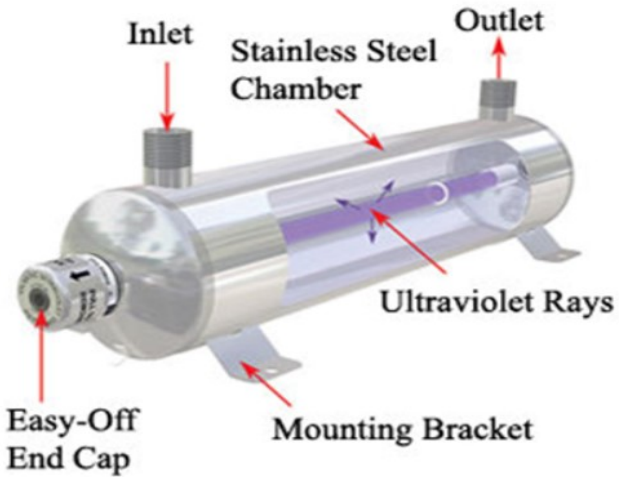

Figure 4: Water Disinfection using UV (javapoint.com)

LEDs are commonly used in indoor settings. LED arrays could be used instead of LDs for shorter UV communication connections (less than one kilometre). Because UV wavelengths are divided into three groups ranging from (200 to 400) nm, higher wavelengths near the upper limit of this range will have higher output optical power than lower wavelengths. LEDs can be used for data exchange in addition to a variety of other applications such as digital printing and UV curing. UV curing is suitable for coating, decorating, and 3D printing in addition to digital printing.

Since crystal advances gained power and chip packaging and processing technologies were developed, the external quantum efficiency of UV-LEDs has significantly increased, particularly between (350 to 400) nm [42]. The quantum efficiency plot for UV-LEDs shows that as the wavelength increases, so does the quantum efficiency. According to [42], there are three possible reasons for an increase or decrease in external quantum efficiency, all of which are related to crystal improvement.

2.2 Ultraviolet Light Detectors

Instruments that measure the amount of ultraviolet or visible light absorbed by sample molecules are known as detectors. Because different molecules have absorption peaks at different wavelengths, they are used for analyte identification and detection in samples. A detector is an important tool in UV-Visible communication because it converts light into proportional electrical signals, which provide the response of a spectrophotometer.

Detectors used in UV communication are currently classified into five types, namely:

- Phototube
- Photo Multiplier Tube
- Diode Array Detector
- Charge Couple Device
- APD Detector

In this study, we used an APD detector with a wavelength range of 200nm to 1000nm for UV light communication. Because UV LEDs have a wavelength of 410 nm, APD detectors detect light more efficiently than other detectors.

2.2.2 Phototube

A phototube is also referred to as a photoelectric cell. A phototube is made up of a light-sensitive cathode and an anode that are enclosed in an evacuated quartz envelope. Between the two electrodes, a potential difference of about 100 V is applied. A photon entering the tube strikes the cathode, causing an electron to be ejected, which strikes the anode, causing current to flow. The phototube's response is affected by the wavelength of the incident light [22].

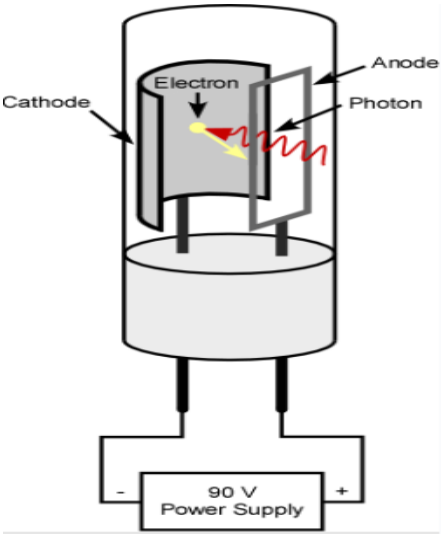

Figure 5: Phototube (Image Courtesy: http://people.whitman.edu/)

2.2.2 Photomultiplier Tube

Photomultiplier tubes (PMTs) are photon detection devices that convert light into an electrical signal by using the photoelectric effect in conjunction with secondary emission. The photoelectric effect causes a photomultiplier to absorb light emitted by a scintillator and re-emit it in the form of electrons. Since then, the PMT has been the primary choice for photon detection due to its high quantum efficiency and amplification [24].

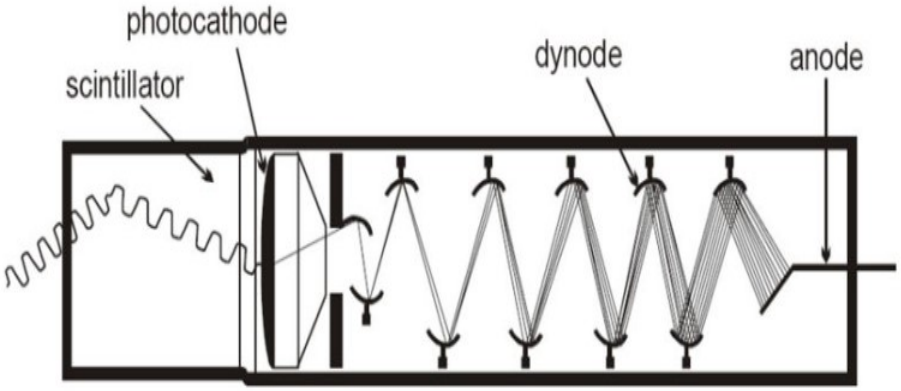

Figure 6: Photomultiplier Tube (Image Courtesy: http://nsspi.tamu.edu/)

2.2.3 Diode Array Detector

A diode array detector is a multichannel photon detector that can measure all wavelengths of dispersed radiation at the same time. An array of silicon photodiodes is accommodated on a single silicon chip. Individual diodes are then scanned for a response. A diode array detector is less sensitive than a photomultiplier tube, but it can measure multiple wavelengths at the same time. Each diode in the array is biased in the opposite direction. When light reaches, charge carriers are produced, which neutralize stored charges with opposite polarities [23].

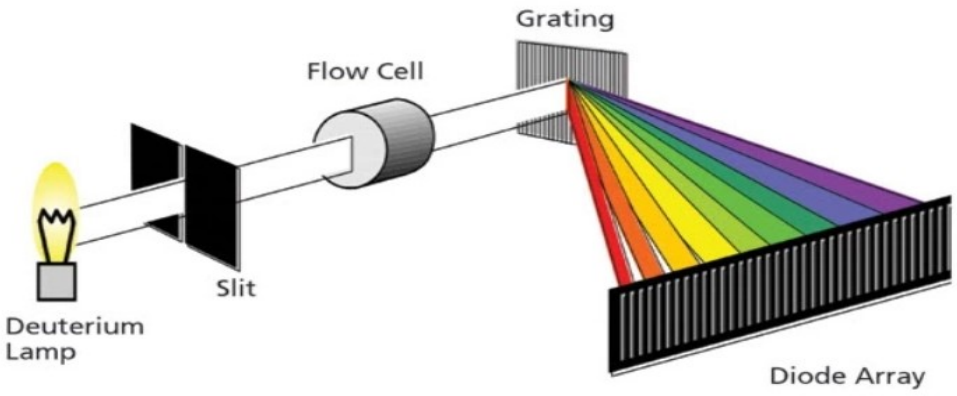

Figure 7: Diode Array Detector [22]

2.2.4 Charge Coupled Device

A charge coupled device (CCD) is a sensitive detector. As a result, it is used to detect signals with extremely low light intensities. It is similar to diode array detectors, but instead of diodes, it uses photo capacitors. They consist of a single or two-dimensional array of photo capacitors. Each photo capacitor is made up of millions of detector elements known as pixels. CCD detectors can detect light from the shortest to the longest wavelengths at the same time. CCD detectors have less noise and greater sensitivity than diode array detectors [23].

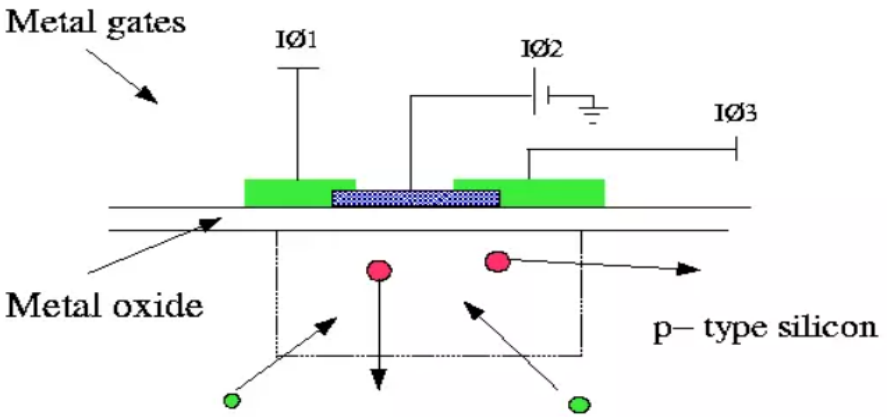

Figure 8: Charge coupled device detector [23]

2.2.5 APD Detector

Si avalanche photodetectors (APDs) outperform standard PIN detectors in terms of sensitivity and noise performance. This APD is appropriate for low-light applications. Avalanche photodetectors, in general, use an internal gain mechanism to increase sensitivity. A strong electric field is created by applying a high reverse-bias voltage to the diode. When an incident photon generates an electron-hole pair, the electron is accelerated by the electric field, and secondary electrons are generated by collision ionization.

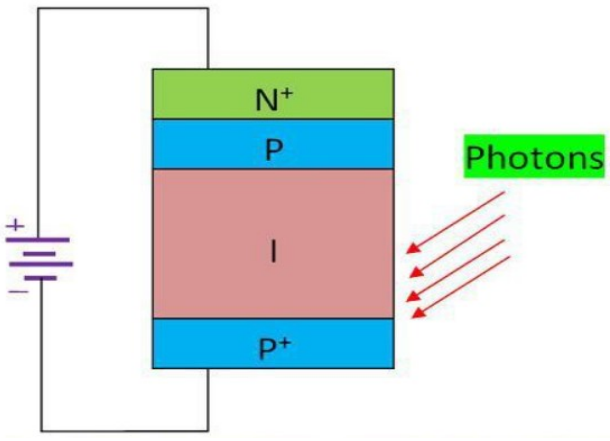

Figure 9: APD Detector (www.electronicscoach.com)

2.4 Application Areas for UV Communication

The advancement of light sources, particularly visible light-emitting diodes (LEDs), has greatly aided the development of VLC. UVC is a novel communication technique that uses UV radiation to transmit signals that are scattered and reflected by particles and aerosols in the air. Its transmission range can be extended up to several kilometers regardless of ground topography. In comparison to traditional wireless communication, UVC has several distinguishing characteristics that make it a promising communication technique for future applications. Traditional wireless communication requires a clear communication channel between transceivers, whereas UVC can easily overcome these obstacles through scattering and reflection. The UV radiation used in communication is also known as solar-blind radiation, and it has a wavelength range of 200-280 nm in the DUV spectrum [25].

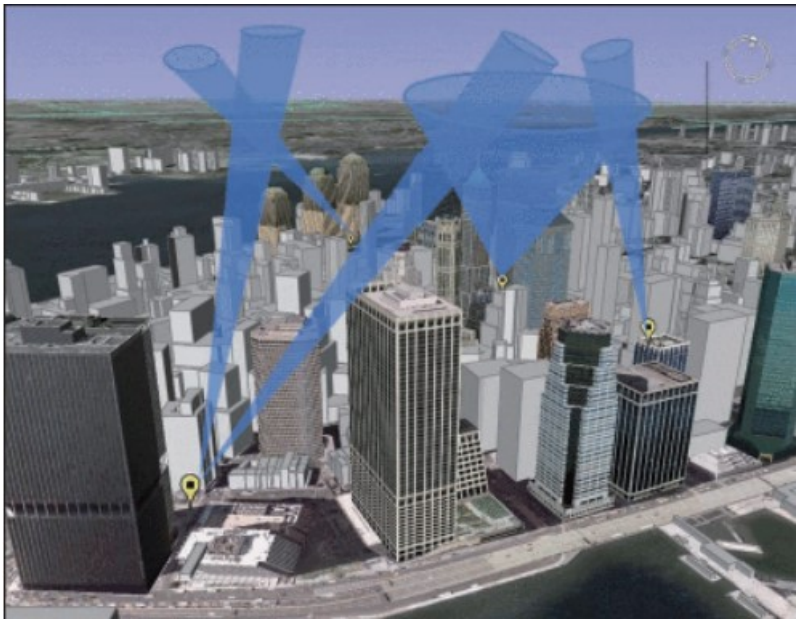

Figure 10: An example of UV communication system [25]

Furthermore, the power of Deep UV radiation decreases exponentially with transmission distance, limiting its propagation and making it an ideal option for short-range communication. UVC can be used as an alternative to traditional wireless communication in radio-silent scenarios.

The ability to communicate in difficult conditions using Flying Ad Hoc Networks (FANET) necessitates the use of non-electronic means of communication. In the absence of line-of-sight between FANET network nodes, optical communication in the UV-C range is used. The general scheme of the UV-C range optical transmitter and receiver is considered, as well as a review of the components required for its implementation, taking into account the application possibility in highly mobile small-sized UAVs. Physical and channel level parameters critical for network performance are revealed as a result of the analysis of FANET networks with UV-C channels [26].

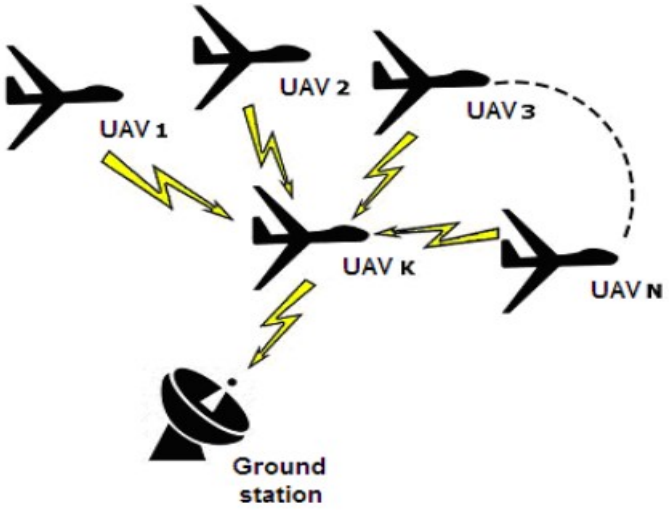

Figure 11: NLOS UV communication channel with UAV [26]

Because the UVC band is a member of the solar-blind ultraviolet band, it has military applications such as short-range ultraviolet security communication, ultraviolet interference, and ultraviolet warning technology. UV communications

could be beneficial to friendly forces while remaining undetectable to adversaries. The researchers intend to investigate four scenarios involving the positioning of the UV transmitter, the intended receiver, and the enemy detector. Both the friendly receiver and the adversary detector are visible to the transmitter. Although the friendly receiver is visible, the adversary detector is not (Best case). Although the adversary's detector is visible, the friendly receiver is not (Worst case). Neither the friendly receiver nor the adversary detector is visible [27].

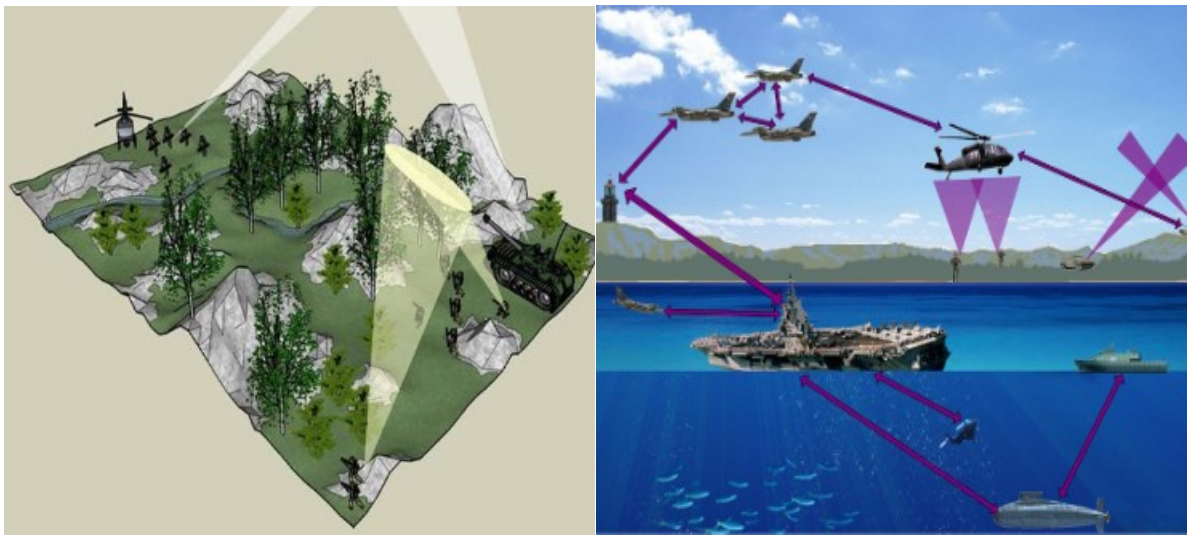

Figure 12: An example of UV communication for Military Use [28]

Chapter 3

NOMA-OFDM Proposed System

3.1 Non-Orthogonal Multiple Access (NOMA)

The concept of non-orthogonal multiple access (NOMA) for future 5G networks. All current cellular networks combine orthogonal multiple access (OMA) techniques like time division multiple access (TDMA), frequency division multiple access (FDMA), and code division multiple access (CDMA). TDMA-based networks necessitate precise synchronization, which can be difficult, particularly in the uplink. Information for each user is assigned to a subset of subcarriers in FDMA implementations such as orthogonal frequency division multiple access (OFDMA) [29].

NOMA is fundamentally different from these multiple access schemes, which provide users with orthogonal access in time, frequency, code, or space. NOMA employs superposition coding at the transmitter, allowing the successive interference cancellation (SIC) receiver to distinguish between users in both the uplink and downlink channels [29]. For two users, user1 and user2, we used the NOMA technique.

- **Non-Orthogonal Multiple Access (NOMA) at Transmitter and Receiver**:

All of the individual information signals are superimposed into a single waveform at the transmitter site. The base station superimposes the information waveforms for its serviced users during the NOMA downlink. We assumed that User 2 is closest to the base station and User 1 is farthest away. We used power coefficient to perform NOMA techniques on each user's raw data bit. The NOMA encoding scheme allocates different power values for different users within each sub-band in the NOMA system. Furthermore, NOMA-OFDM is a versatile scheme that allows users to transmit data

across multiple sub-bands. In practice, most NOMA schemes assume that at most two users will be multiplexing through the same degree of freedom (DOF).

$$s[k] = \sqrt{\alpha P} \cdot s_1[k] + \sqrt{(1-\alpha)P} \cdot s_2[k] \ldots\ldots\ldots \quad (1)$$

Consider equation (1), and suppose User 1's channel condition is better than User 2. User 1's power allocation factor is, and the total power of S1[k] and S2[k] is P. S[k] denotes the linear superposition of the two users' signals. The individual information conveyed by the OFDM waveform is denoted by S[k].

These optical signals can be received as a total received signal by a single APD detector on the Rx side. And the received signal y is denoted as,

$$y = h_1\sqrt{P_1}x_1 + h_2\sqrt{P_2}x_2 + w\ldots\ldots\ldots \quad (2)$$

where x 1 and x 2 represent the transmitted signals of User 1 and User 2, respectively, and y represents the total received signal at the Rx. The h 1 and h 2 values represent the Rayleigh fading coefficients of User 1 and User 2 between Rx and Tx. P denotes the power of the respective users. And w stands for Additive White Gaussian Noise [31].

- **Signal Cancellation Interference (SIC) technique:**

Signal Interference Cancellation (SIC) decodes each signal one by one until the desired signal is found. Figure 2 depicts the concept. The information signals are superimposed on the transmitter in the illustration. All of these signals are included in

the received signal at the SIC receiver. The first signal decoded by SIC is the strongest while others act as interference. The first decoded signal is then subtracted from the received signal, and if the decoding is perfect, the waveform with the remaining signals is obtained accurately. The process is iterated by SIC until the desired signal is observed [32].

At the receiver side, the successive interference cancellation (SIC) method is used, and the optimal detection order is the ascending order of channel gain. Without loss of generality,

| H1[k] | > | H2[k] |

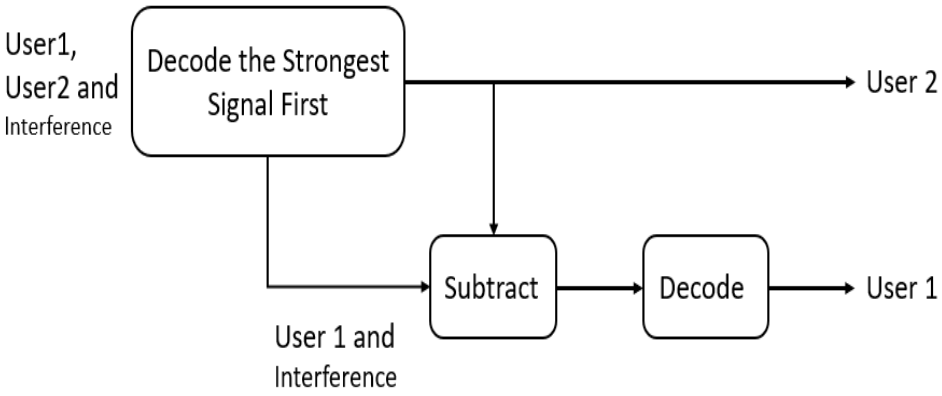

Figure 13: Successive Cancellation Interference [29]

The signals of User 1 are detected first by treating the signals of User 2 as noise at User 1's receiver. In other words, User 2 is no longer permitted to perform SIC. For the receiver at User 1, the interference from the signals at User 2 must be detected, and the detected interference must then be reconstructed and subtracted. Following that, User 1 detects its own signals.

$$y_1 = \sum_{i=1}^{s} H_1^H x_i + n_1 \qquad \text{.....(3)}$$

Were,

$$x_i = \sqrt{P_i} \cdot s$$

where H is a channel effect. n1 is noise (additive white Gaussian Noise) x_i is a Power allocation Coefficient*User of Signal [32].

3.2 Orthogonal Frequency Division Multiplexing (OFDM)

OFDM is a digital multi-carrier modulation scheme that extends the concept of single subcarrier modulation by utilizing multiple subcarriers within the same single channel. Rather than transmitting a high-rate data stream with a single subcarrier, OFDM employs a large number of closely-spaced orthogonal subcarriers being sent in parallel. At a low symbol rate, each subcarrier is modulated with a conventional digital modulation scheme (such as QPSK, 16QAM, and so on) [33].

In this research, we used the Fast Fourier Transform (FFT) to implement OFDM. The concepts used in the simple analog OFDM implementation can be extended to the digital domain by combining digital signal processing with Fast Fourier Transform (FFT) and Inverse Fast Fourier Transform (IFFT). These transforms are significant in the context of OFDM because they can be thought of as mapping digitally modulated input data (data symbols) onto orthogonal subcarriers. The IFFT converts frequency-domain input data (complex numbers representing modulated subcarriers) to time-domain output data (analog OFDM symbol waveform) [33].

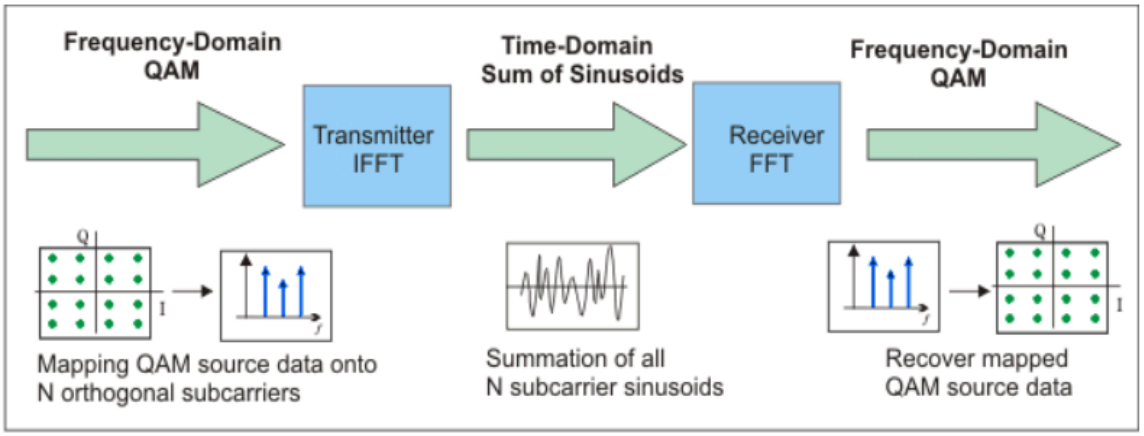

Figure 14: Simplified OFDM System Block diagram [34]

The input bits in an implemented OFDM system are mapped to source data symbols that are a complex number representing the modulation constellation point. The transmitter considers these complex source symbols as if they are in the frequency domain, and they are the inputs to an IFFT block that transforms the data into the time domain [34].

3.3 Modulation Schemes

The process of encoding information from a message source for transmission is known as modulation. Analog modulation and digital modulation are the two types of modulation. Analog modulations include amplitude modulation (AM), frequency modulation (FM), and phase modulation. Quadrature Phase Shift Keying (QPSK), Minimum Shift Keying (MSK), Frequency Shift Keying (FSK), Quadrature Amplitude Modulation (QAM), and other digital modulations. To improve the overall performance of wireless communication systems, the performance of all modulation techniques is both coded and uncoded through various simulation processes under MATLAB software.

3.3.1 Phase Shift Keying (PSK)

PSK is a digital modulation process that sends data by changing the phase of a constant frequency reference signal. It's common in wireless LANs, RFID, and Bluetooth communication. PSK employs a limited number of phases, each with its own unique pattern of binary digits. The demodulator, which is customized to the modulator's symbol set, determines the phase of the received signal and maps it back to the symbol.

"Binary phase-shift keying" (BPSK), which uses two phases, and "quadrature phase-shift keying" (QPSK), which uses four phases, are two common examples, though any number of phases can be used. Because the data to be transmitted is typically binary, the PSK scheme is typically designed with the number of constellation points being limited a power of two [36].

3.3.2 Binary Phase Shift Keying (BPSK)

The binary information in BPSK is in the two-phase shifts of the carrier signal, which correspond to a binary 0 or a binary 1. The carrier signal has two amplitude levels. These two phases are opposite each other by 180 degrees. As a result, these two waveforms are antipodal. Only by allowing more than two waveforms for information transmission can the error probability be reduced [35]. First, the NRZ encoder converts these digital bits into impulses to give them a sense of time. After that, the NRZ waveform is created by up sampling these impulses. Following that, multiplication with the carrier is performed to generate the modulated BPSK waveform.

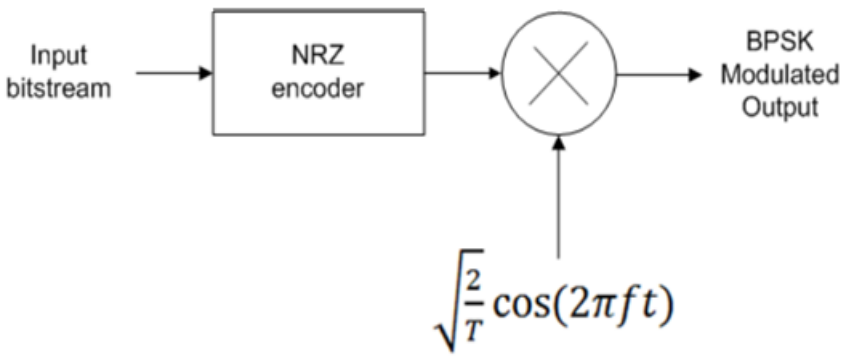

Figure 14: BPSK Modulator (drmoazzam.com)

3.3.3 Quadrature Phase Shift Keying (QPSK)

The quadrature phase-shift keying (QPSK) technique is more efficient than ASK, PSK, and FSK in terms of data transmission rate and bandwidth utilization, and it does not affect bit error rate at the expense of a more complex receiver structure.

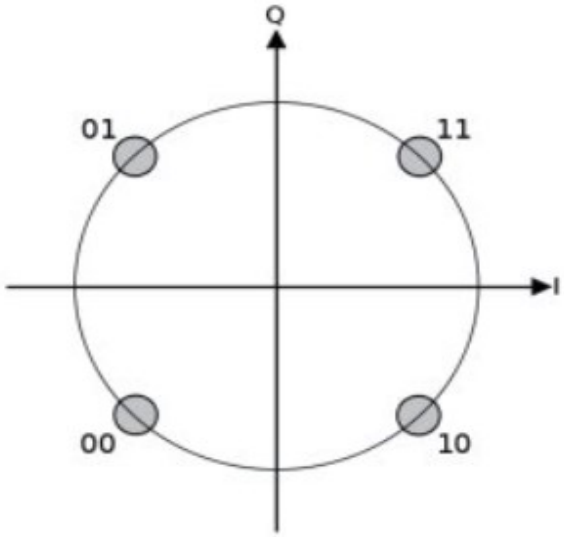

Figure 15: QPSK Constellation(www.researchgate.net)

QPSK uses two carriers of the same frequency that are orthogonal to each other to transmit two bits at a time with equal bandwidth and bit error rate to PSK. Because

QPSK transmits two bits at a time, there are four possible symbols: 00, 01, 10, and 11 [37]. We used QPSK modulation to compute OFDM data in this study research.

3.3.5 Quadrature amplitude modulation (QAM)

Quadrature amplitude modulation (QAM) is a type of digital modulation that uses the amplitude modulation (AM) analog modulation scheme to transmit two analog message signals or two digital bit streams. QAM comes in a variety of forms, the most common of which are 16QAM, 32QAM, 64QAM, 128QAM, and so on [38].

There are various types of an M-ary digital modulation techniques that are used in many communication system applications such as digital radio and digital video broadcasting, among others [39].

3.4 Channel Effect

The transmission of information between transmitters and receivers necessitates the use of a physical transmission medium or a free space medium, which is referred to as a communication channel. In wireless communication, channels are classified as Additive White Gaussian Noise (AWGN) or fading channels. Rayleigh and Rician channels are two types of fading channels [39]. In this research, the noisy channel estimates by Additive White Gaussian Noise and channel fading affected the signal due to the distance between Users 1 and 2 as predicted by Rayleigh channel fading.

3.4.1 Additive White Gaussian Noise (AWGN)

In wireless communication, the AWGN channel model provides information in a single loss that is a linear addition of wide band or white noise with a constant spectral density expressed as watts per hertz of bandwidth and a Gaussian amplitude

distribution. Interference, fading, nonlinearity, frequency selectivity, and dispersion are not accounted for in the model. It does not experience fading, which is what a carrier-modulated signal does over certain propagation media [35]. Figure 16 depicts the AWGN Channel Model Block Diagram.

$$R(t) = T(t) + n(t) \quad \text{..... (4)}$$

where the received signal R(t) is equal to the, the transmitted signal T(t) plus the background noise n(t) [39].

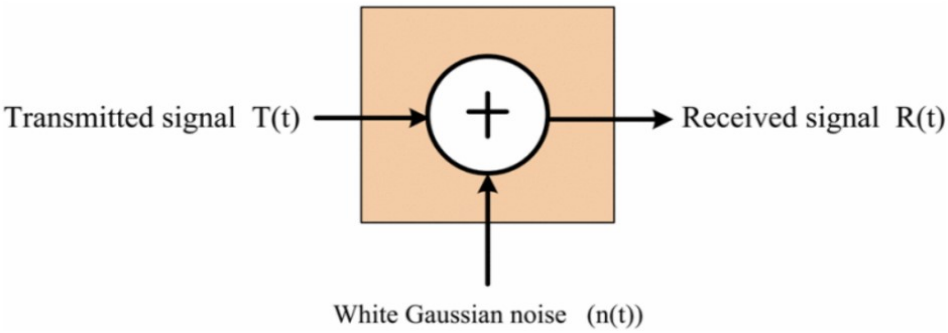

Figure 16: AWGN Channel Model

3.4.2 Rayleigh Fading Channel

Rayleigh fading is also referred to as a Non-line of Sight (NLOS) channel. The distribution in Rayleigh channel fading is caused by multipath with or without the Doppler effect. When the transmitted signal weakens in a multipath case, the received signal is the sum of several components that are reflected from obstacles such as buildings. There are numerous other ways for the signal to reach the receiver in this channel scheme. When the signals arrive at the receiver, the overall signal is a combination of all the signals received via the host [39].

3.5 Proposed System

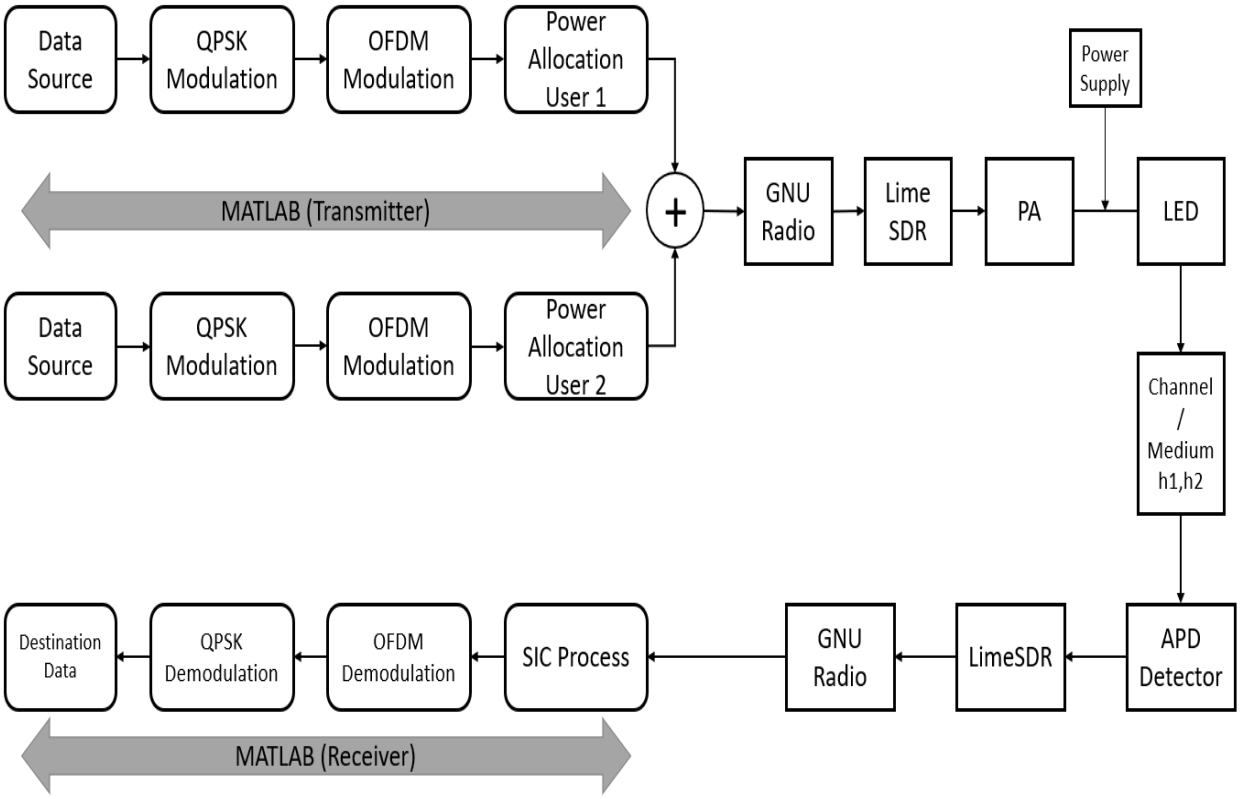

Figure 17: Block diagram for Proposed Scheme

We defined the entire experimental setup in this section. Figure 3 depicts the flow diagram of the proposed NOMA-OFDM communication system scheme. LimeSDR hardware, GNU Radio, and MATLAB software are used in the experiment. As shown, all signal processing, including mapping, IFFT, and so on, will be done in MATLAB first. After generating the OFDM signal in MATLAB, we will save it in a.wav file. We can examine the.wav file using GNU Radio Software (audio file). Obtain the OFDM signal from the file and send it to the LimeSDR, which is connected to GNU Radio. This software is used to configure the LimeSDR's transmitter (TX port) and receiver (RX port).

The signal is then sent to the Power Amplifier (PA) via the LimeSDR's TX port, where the OFDM signal is amplified. To make the signal non-negative, the amplified

signal and direct current will be combined using a bias tee. The electrical signal will then be transmitted to two distinct UV-LEDs, where it will be converted into an optical signal. These two LEDs will transmit their signals at the same time, but the signals will be different. These signals will be intercepted by a single APD detector. The total optical signal received through each LED will be detected by this APD detector and converted into an electrical signal. The signal will then be sent back to GNU Radio via the LimeSDR's Rx port. We then use GNU Radio to save the received signal as a.wav file.

Finally, we used MATLAB to read the received.wav file. Then, in this received signal, we can determine the Successive Interference Cancellation (SIC). Because this signal contains a lot of noise, OFDM and QPSK demodulation will be used. Following that, we will use the SIC method to differentiate these two signals and calculate the BER to investigate the overall performance of the NOMA-OFDM communication system.

Chapter 4
Introduction of Experimental Devices

1. MATLAB

MATLAB (Matrix Laboratory) is a multi-paradigm software package that combines a desktop environment for iterative analysis and design processes with a programming language that directly represents matrix and array mathematics. MATLAB supports matrix manipulation, function and data plotting, algorithm implementation, user interface creation, and interfacing with programs written in other languages.

In this research, we used the MATLAB R2022a version. MATLAB is used for all signal processing, including mapping, IFFT, modulation, and demodulation of generated signals.

2. GNU Radio

GNU Radio is a free software development toolkit that contains signal processing blocks that can be used to build software-defined radios and signal-processing systems. It can be used with external RF hardware to create software-defined radios, or it can be used in a simulation-like environment without hardware. GNU Radio is used to power the LimeSDR hardware in this study. The.wav file is examined using GNU Radio Software (audio file). This software is used to configure the LimeSDR's of the transmitter (TX port) and receiver (RX port) of the LimeSDR.

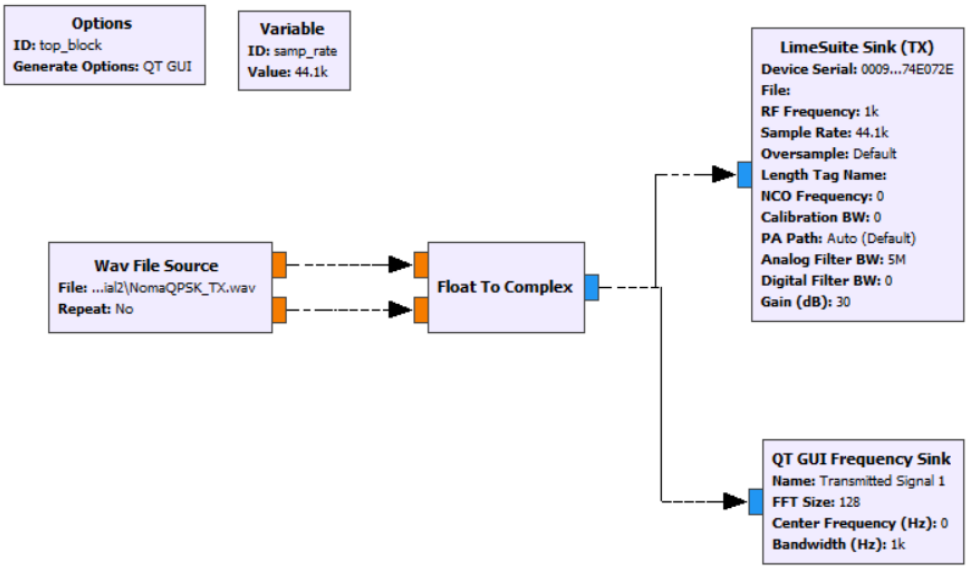

Figure 18: Example of Transmitter file in GNU Radio

3. LimeSDR

LimeSDR is a low-cost, open source, apps-enabled software defined radio (SDR) platform that can support practically any wireless communication standard. Figure 19 illustrates the LimeSDR's numerous Tx and Rx ports, as well as its single USB interface. In which the USB interface is connected to the computer, allowing the GNU radio on the computer to drive and control the LimeSDR.

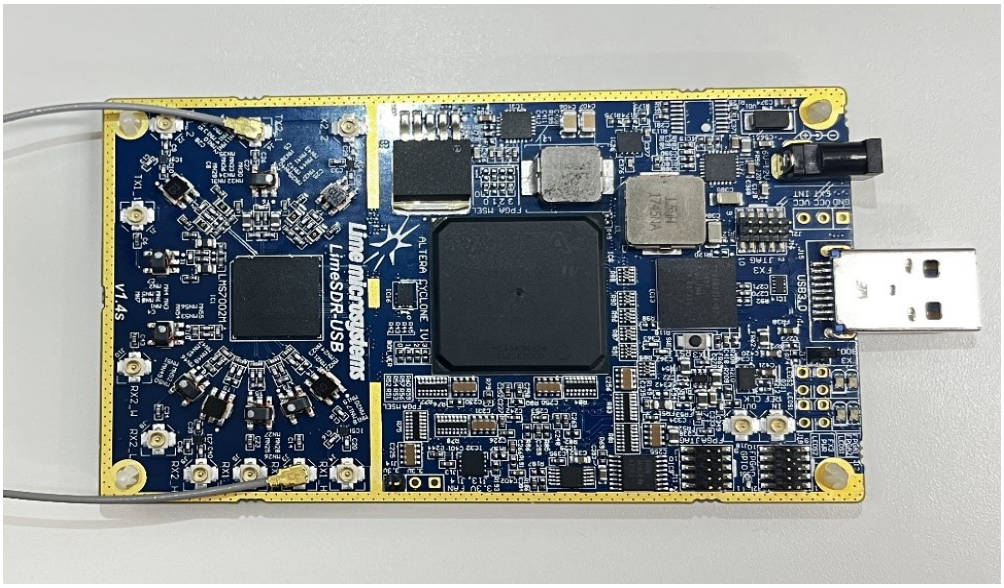

Figure 19: LimeSDR Board

4. Power Amplifier

A power amplifier's function is to increase the power level of the input signal. It must deliver a large amount of power while also handling a large current. Following the conversion of an audio signal to an electrical signal, several voltage amplifications are performed, followed by power amplification of the amplified signal. Following the conversion of an audio signal to an electrical signal, several voltage amplifications are performed, followed by power amplification of the amplified signal. It is the power amplifier with a 20dB gain and a frequency range of 5-6000MHz, as illustrated in Fig. 20.

Figure 20: Power amplifier

5. Bias Tee

Bias tees are components that provide DC currents or voltages to bias RF circuits. A bias tee is a three-port connector. The device's structure is depicted in figure 21(b) below. At Port 1 of the Bias Tee, a signal consisting of RF + DC is incident. The capacitor

prevents all DC signals from reaching Port 2 and only allows AC/RF signals to pass through.

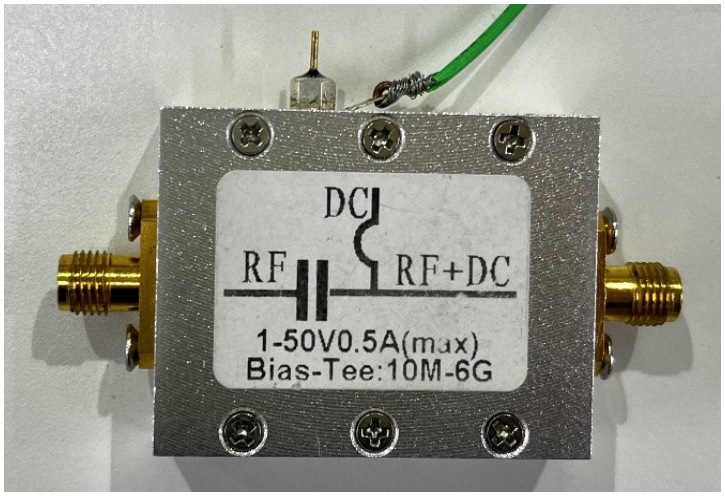

Fig 21(a): Bias-Tee

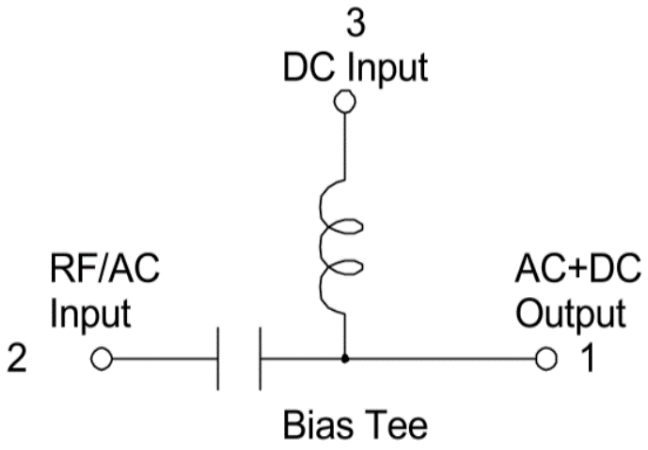

Fig 21(b): Structure of Device (awrcorp.com)

The Bias-Tee, as shown in Fig. 21(a), can add a 1-50V DC bias to the transmitted signal. The signal's frequency range is 10MHz-6GHz.

6. UV-LED band A

We used UV-LED of band A in this research, as shown in figure 21(a), because UV-band-A has lower propagation losses than UV-band-C while having ambient lighting noises. Figure 22 shows a UV-A LED with a wavelength of 400 nm to 410 nm 22 (b).

Figure 22(a): UV-LED

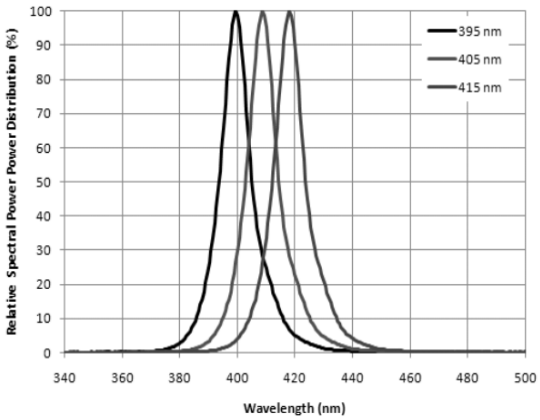

Figure 22(b): Wavelength(nm) [40]

7. Power Supply:

The power supply is represented in Figure 23. It has two power supply ports and can supply two different direct currents at the same time, making it ideal for this experiment. It has a supply voltage range of 0-20V. In this experiment, a DC bias of 3V is sufficient.

Figure 23: Power Supply

8. APD Detector

Figure 24 illustrates the experiment's photodiode. It is a Si avalanche Photodetector from THORLAB, model APD430 A2/M, with a detection range of 200nm to 1000nm. We can detect the optical signal transmitted by the LED and convert it to an electrical signal in the time domain by connecting this photodiode to the LimeSDR's Rx port. The LimeSDR will transmit this electrical signal back to GNU Radio.

Figure 24: APD Detector(200nm-1000nm)

Chapter 5

Experimental Results and Discussion

In this section, we present experimental results for the Ultraviolet communication system under consideration. We have considered system and channel parameters which are provided in Table I.

Table I: Parameters of the Simulation

Parameters	Values
Number of Data bits	64
Number of Sub carriers (M)	4
Cyclic Prefix Length	32
Count of Carriers	128
Symbols per carrier	160
Sample Rate	44100
Power Coefficient of User 1 (α1)	0.75
Power Coefficient of User 2 (α2)	0.25
IFFT	128
DC Current	3V
Modulation Schemes	PSK QPSK QAM

First, we generated a random data source of length 64 that will be transmitted. Figure 25 illustrates the randomly generated data.

The interval [0 Amplitude] or [Amplitude 0] contains a uniform distribution of random integers in the random signal for positive and negative amplitudes, respectively. Random signals are advantageous because they can uniformly excite the system at all frequencies up to the Nyquist frequency.

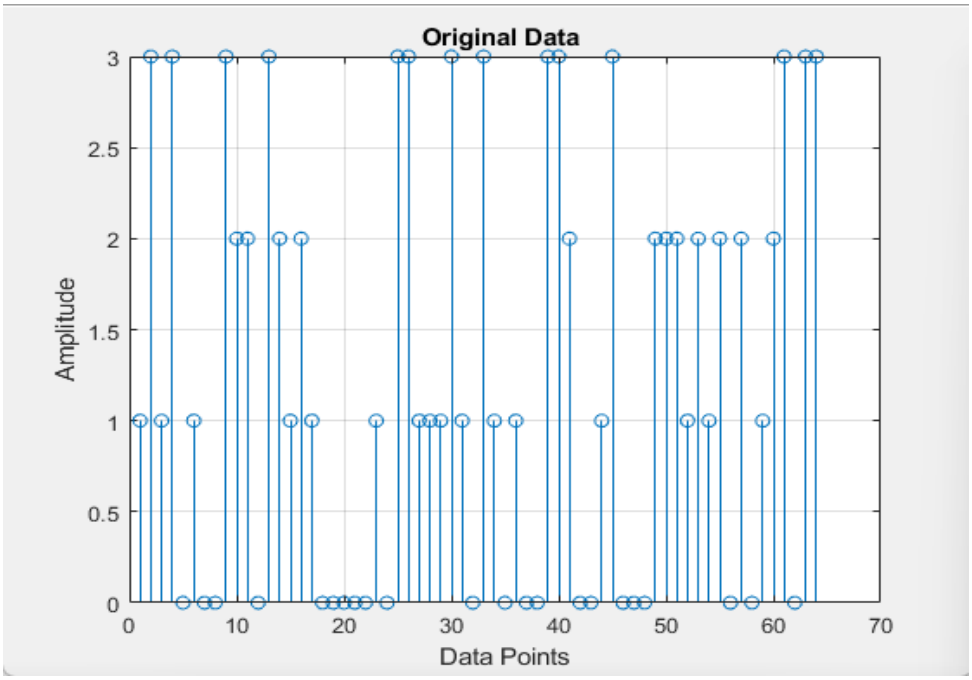

Figure 25: Generated Random data

The QPSK modulation technique is then computed on each user's raw data. At a low symbol rate, each subcarrier is modulated using a traditional 16QAM or QPSK digital modulation technique. The OFDM carrier signal is the sum of one or more OFDM symbols, each of which has four orthogonal subcarriers that are independently modulated using quadrature amplitude modulation (QPSK). The main RF carrier is modulated using this composite baseband signal.

Rather than transmitting a high-rate data stream with a single subcarrier, the series data stream is converted into four parallel data streams to form four subcarriers. Figure 26 depicts the four generated sub-carriers.

When orthogonal subcarriers are used, more subcarriers can be used per bandwidth, increasing spectral efficiency. In a perfect signal, orthogonality prevents overlapping carriers from interfering with one another. Inter-subcarrier interference, for instance, is caused by frequency error, which shifts the subcarrier frequencies and causes the spectral nulls to no longer be aligned.

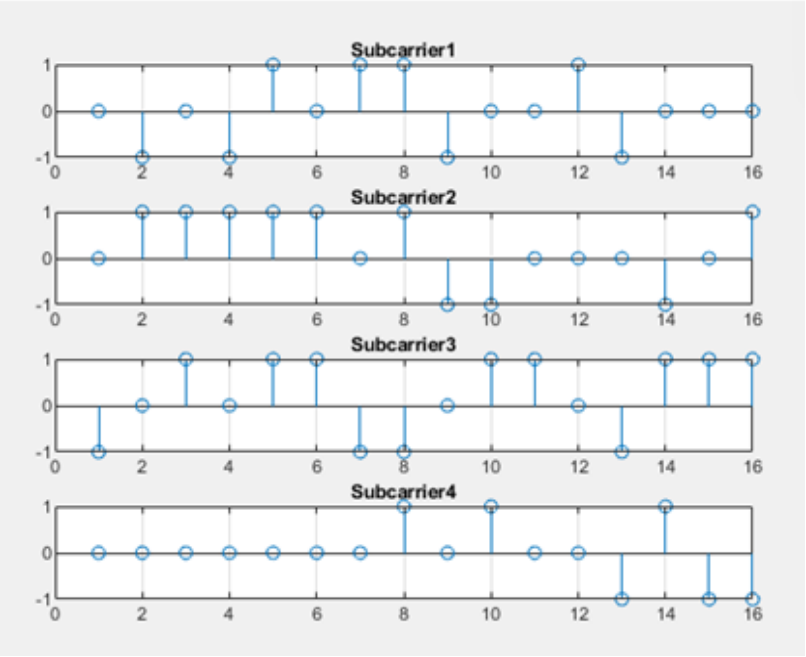

Figure 26: Four Sub-carriers

Following that, we used IFFT to generate sub-carriers. Figure 27 shows the application of IFFT to sub-carriers. The input bits are grouped and mapped to complex numbers representing the modulation constellation point as source data symbols. These complex source symbols serve as inputs to an IFFT block, which converts the data into the time domain and processes it as if it were in the frequency domain.

N represents the number of subcarriers in the system, and the IFFT accepts N source symbols at once. Each of these N input symbols has a symbol period of T seconds. Remember that the output of the IFFT is N orthogonal sinusoids. The frequency of each of these orthogonal sinusoids varies, with DC having the lowest frequency.

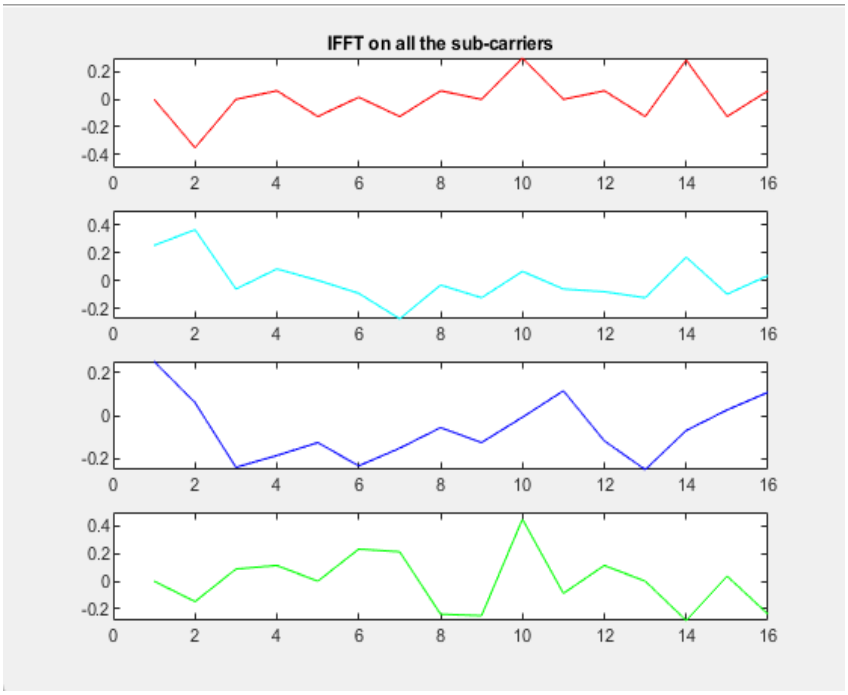

Figure 27: Inverse Fast Fourier Transform on Sub carriers

Then, as shown in Figure 28, a cyclic prefix will be added to IFFT Sub-carriers. The cyclic prefix must be a circular repetition of the IFFT data either before or after the IFFT block, and it must be at least as long as the channel's maximum expected multi-path delay time differential and the maximum timing error between the received data block and the receiver symbol clock. The M/4 is simply a default estimation of this time for several popular channels; additional time may be required.

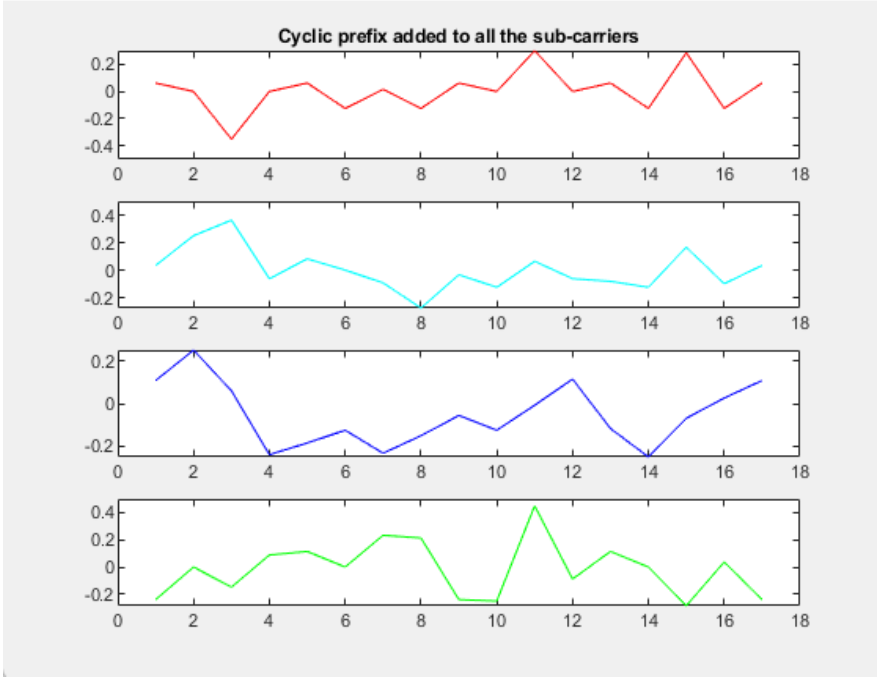

Figure 28: Added Cyclic Prefix

When the IFFT is completely added, the Inverse FFT is computed, resulting in a set of complex time-domain samples representing the combined OFDM subcarrier waveform, as shown in figure 29.

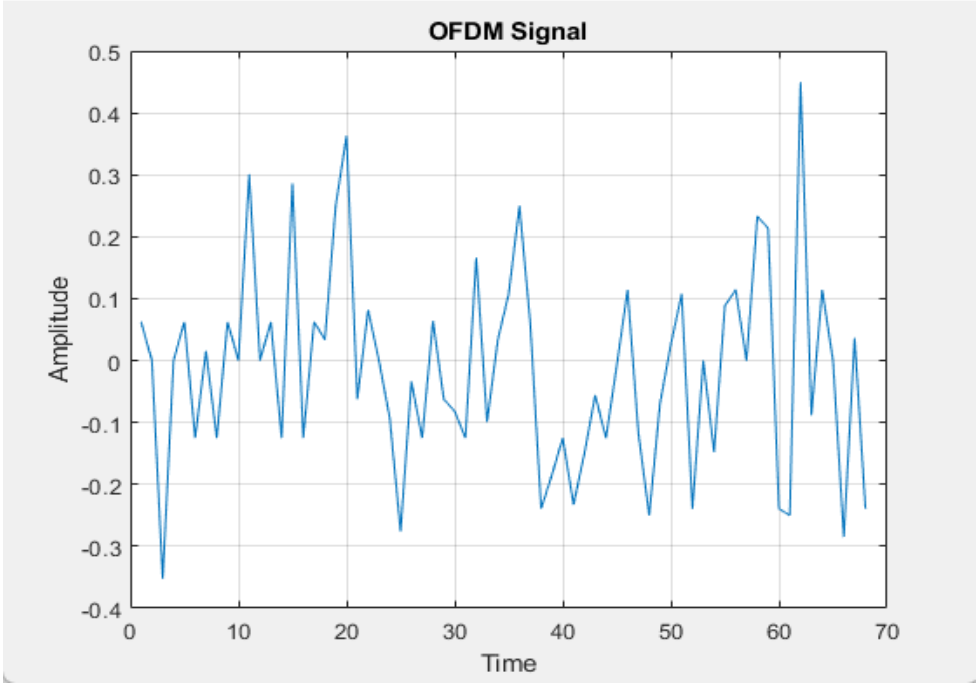

Figure 29: OFDM Signal

Then, utilizing the power coefficient, we execute Non orthogonal multiple access techniques (NOMA). Power distribution is critical in non-orthogonal multiple access (NOMA). Until now, we have utilized fixed power allocation. That is, we set the values of α1 and α2 regardless of channel circumstances. However, there are better approaches to dynamically optimize α1 and α2 depending on channel state information values (CSI). We define fixed power allocation as setting α1=0.75 (for far user) and α2=0.25 regardless of channel condition. This is one method of allocating power. Figure 30 depicts the power allocation waveform for two users, User1 and User2.

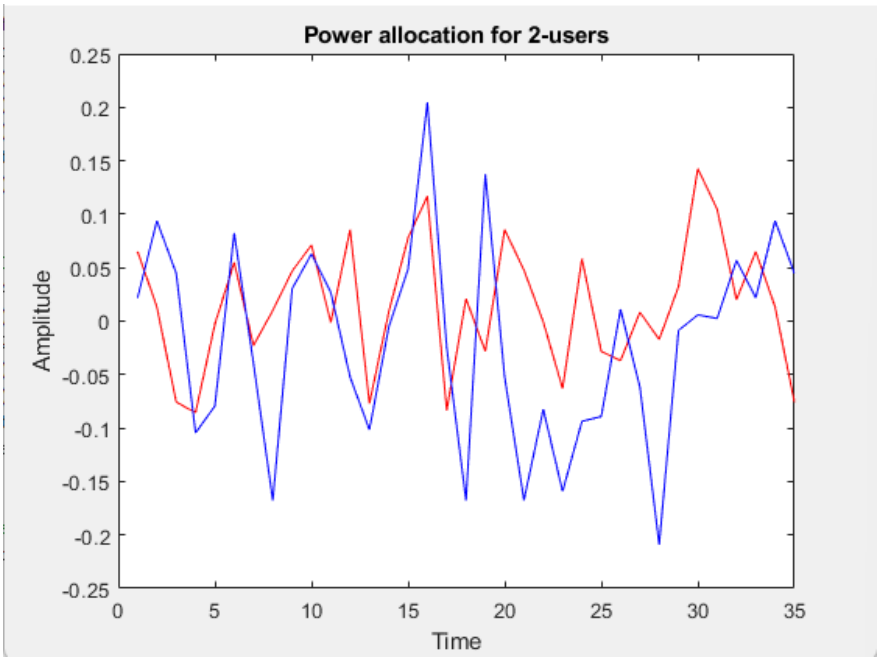

Figure 30: Power allocation

As previously explained in Chapter 3, the NOMA equations We considered in terms of α2 by performing the transformation α2=1−α1. (Because we know that α1>α2 and, α1+α2=1). The benefits of this fixed power distribution approach include minimal calculation and no knowledge of channel state information (CSI). Figure 31 shows the combination of User1 and User2's NOMA waveforms.

This generated NOMA waveform will be sent to the GNU Radio program as a.wav file. Because we can drive LimeSDR devices to generate the signals we require, we use GNU Radio software to read.wav files. The.wav file is examined using GNU Radio Software (audio file). This software is used to configure the LimeSDR's transmitter (TX port) and receiver (RX port).

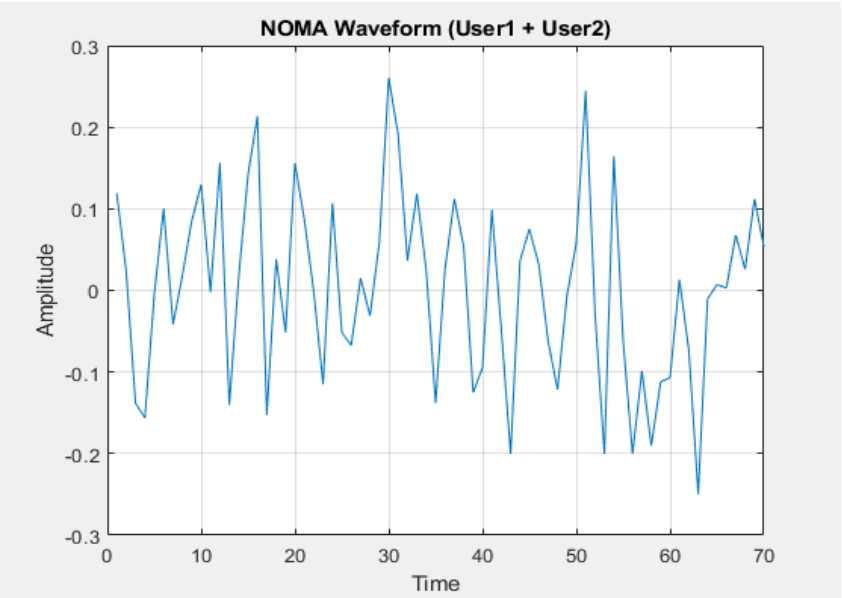

Figure 31: NOMA Waveform

To drive LimeSDR hardware, we used Wav file source, LimeSuite Sink TX-RX, WX GUI FFT Sink, and Wave File Sink block in GNU code, as illustrated in figure 18 (described in chapter 4). Wav file source is a data source created from an audio wave file. To send real-time recording device data, the Wav file source could be converted to an Audio source. At 44100, LimeSuite Sink (TX) is utilized to consume (transmit) samples. WX GUI FFT Sink analyzes FFT of samples created for LimeSuite Sink (TX) consumption, while LimeSuite Source (RX) produces (receives) samples at 44100 rates. The received.wav file is saved using the Wave File sink.

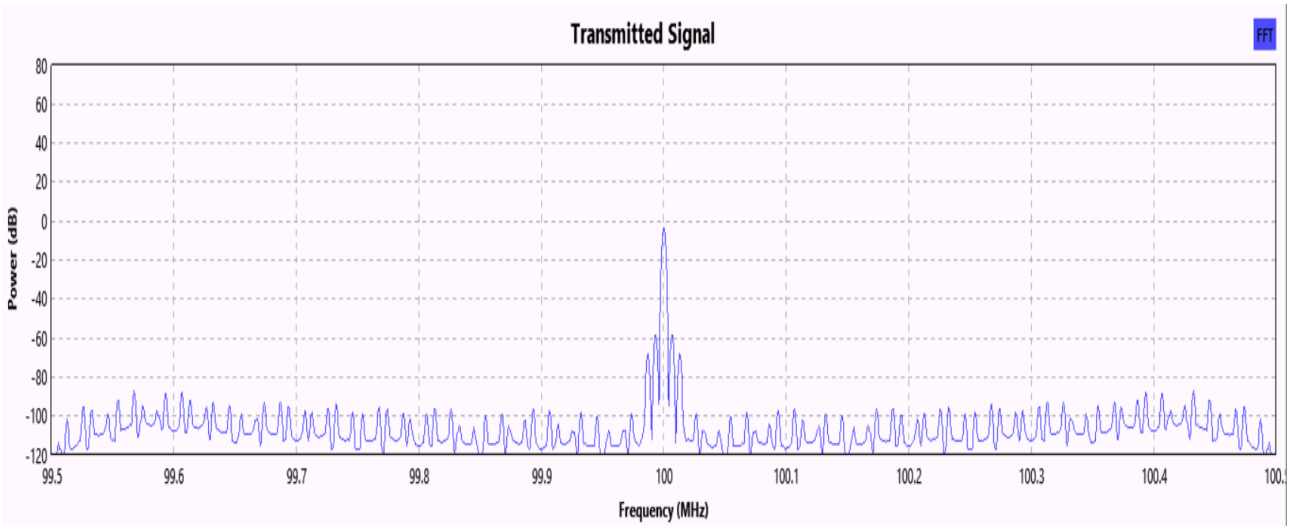

Figure 31: Transmitted Signal

Figure 31 shows the signal delivered in GNU Radio using the LimeSDR TX port. LimeSDR-USB supports RF center frequencies ranging from 100kHz to 3.8GHz. Gain, a call-back function parameter that regulates the TX channel gain, is set to 30 dB. Figure 32 (a) and 32 (b) shows the received signals at 1m and 1.5m distance respectively.

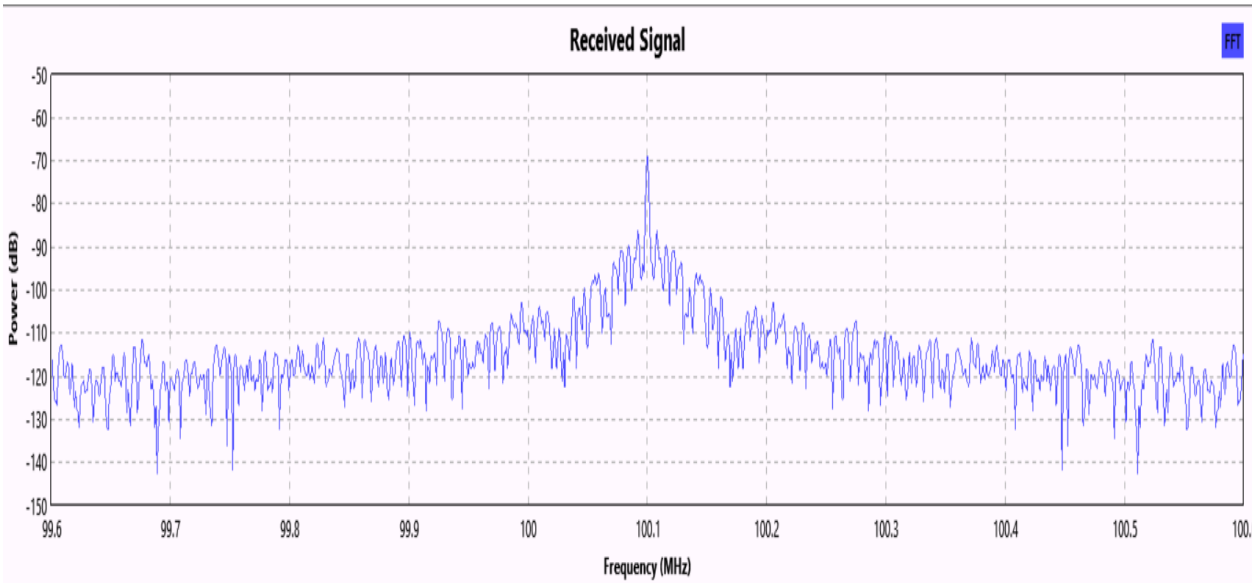

Figure 32 (a): Received Signal at 1m distance

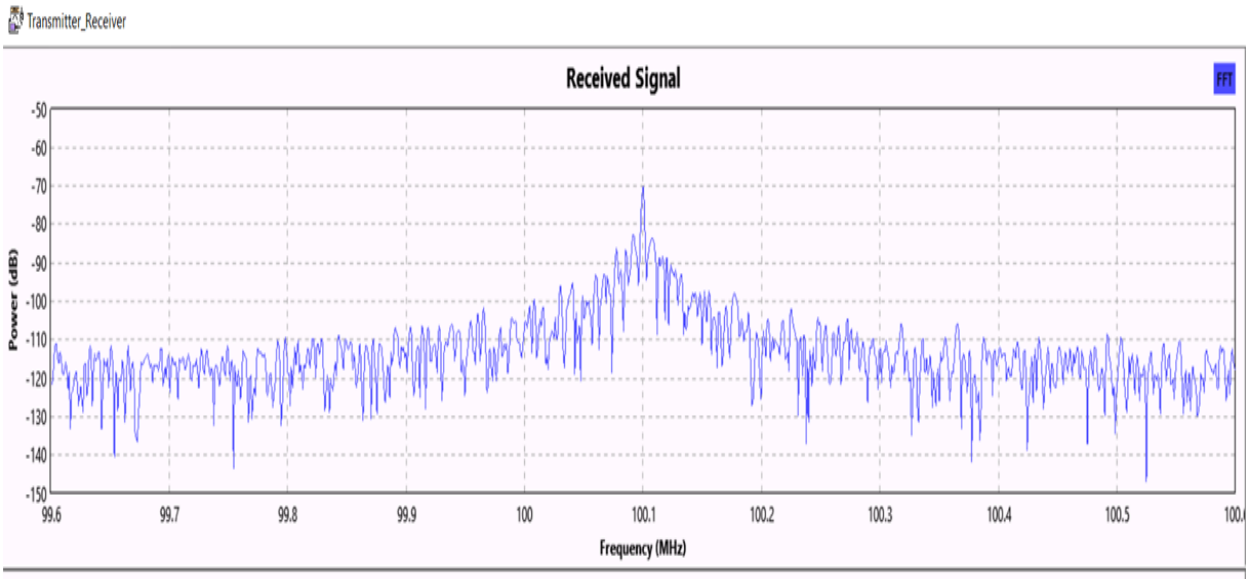

Figure 32 (b): Received Signal at 1.5m distance

Once the hardware experiment is done, we receive a .wav file through LimeSDR port RX in GNU Radio Software. Then we need to convert this .wav file to a mat file in MATLAB. Figure 33 shows the received waveform.

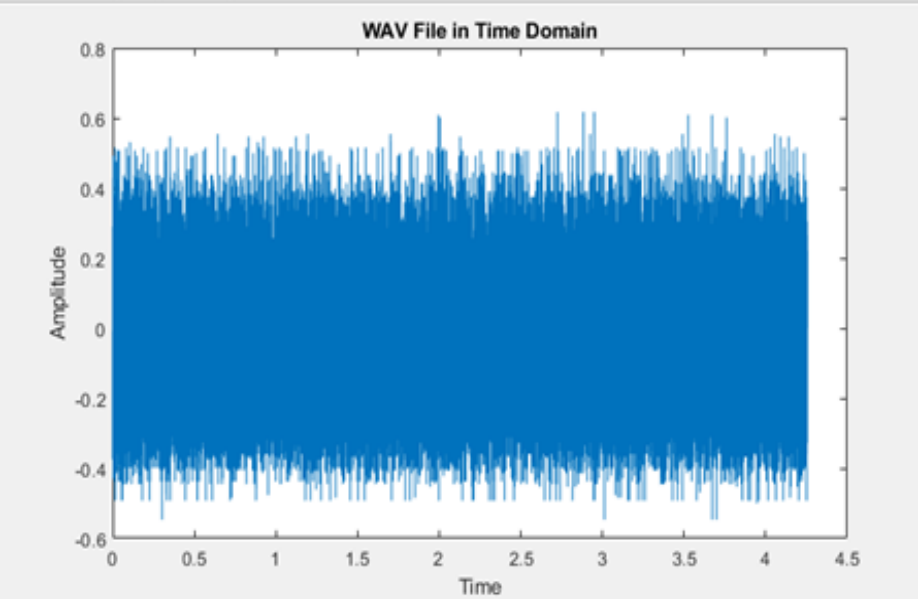

Figure 33: Received Signal of a converted wav file

Figure 31 shows that the received waveform is significantly larger than the transmitted signal. The overall sampled value of the receiver output is very enormous, resulting in incompatibility with the source data. Because the received signal contains various disturbances, it is substantially longer than the original transmitted signal. To compare it to the original data, we must shorten the waveform. The cut waveform is represented in Figure 34.

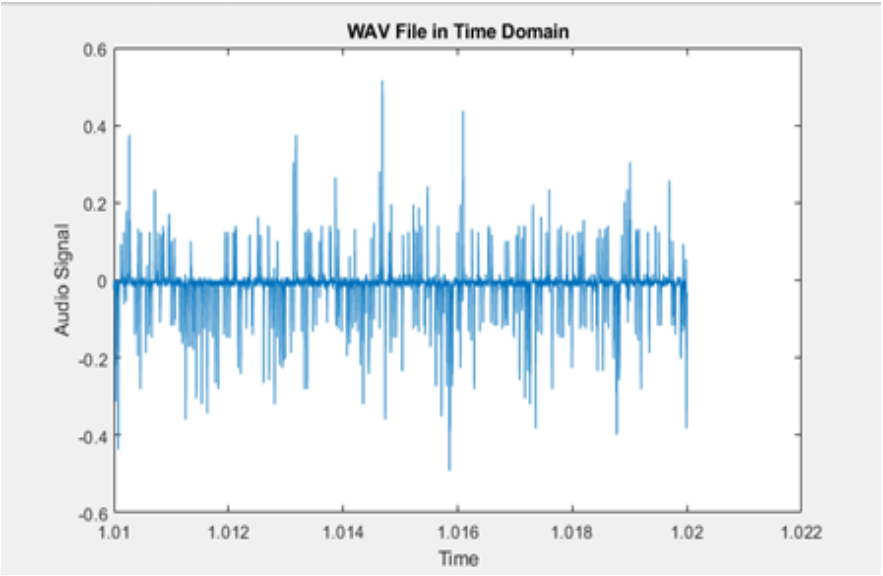

Figure 34: Cut Waveform

To determine the system's overall BER, we must first decode the received signal using the successive interference cancellation (SIC) approach. As previously discussed, the power allocation coefficients $\alpha1= 0.75$ and $\alpha2= 0.25$. According to NOMA principles, the weakest user should be given the most power, while the strongest user should be given the least. As a result, the power allocation coefficients must be arranged as $\alpha1>\alpha2$. We employed QPSK modulation for both users to plot the bit error rate (BER) of a two-user NOMA.

The Base Station (BS) must send QPSK modulated messages to User 1 and User 2, respectively. The BS then transmits the superposition coded signal. Because User 1 has the most power, he will do direct decoding, treating User 2's signals as

interference. Then, in order to remove User 1's data, User 2 must execute sequential interference cancellation. After SIC removes User 1's data, the attainable rate is User 2. Each symbol contains two bits because we are utilizing QPSK modulation. As a result, we will transmit N/2 symbols. We are producing Rayleigh fading coefficients h1 and h2 for each symbol (equation explained in chapter 3, 3.1 section). Modulate each user's message with QPSK. For this, we have used MATLAB's in-built QPSKmod and QPSKdemod, modulator and demodulator objects.

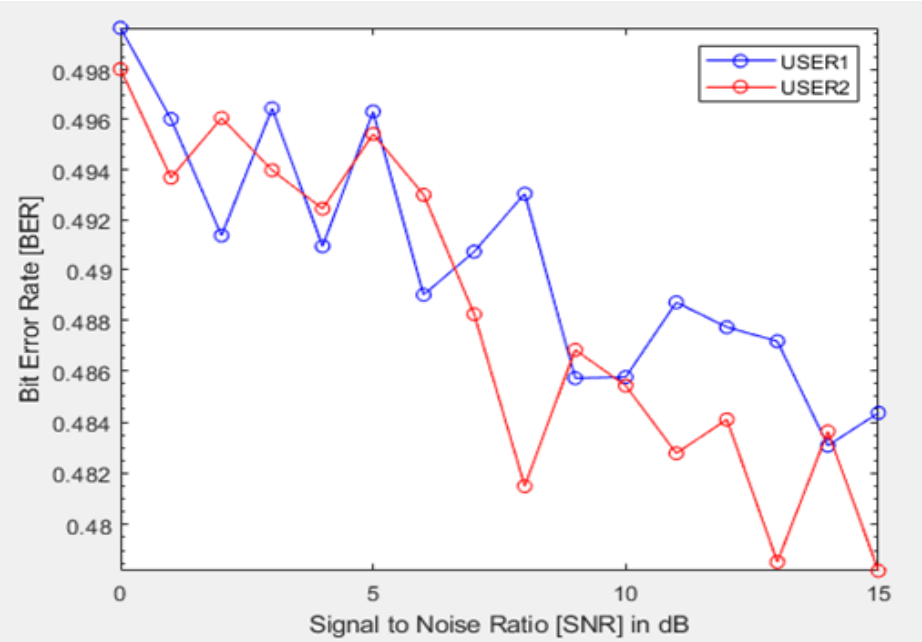

Figure 34: BER using QPSK for User1 and User2

BER is a parameter that provides an excellent indication of a data link's performance. The BER is defined as the percentage of bits that include mistakes divided by the total amount of bits conveyed. BER can be stated mathematically as [39].

$$BER = \frac{\text{Number of bit errors}}{\text{Total number of bits send}} \quad \text{.....(5)}$$

Finally, as illustrated in Figure 34, we may compute BER using the QPSK modulation approach. The Bit Error Ratio (BER) for PSK, 4-QAM, and QPSK modulation schemes was also compared.

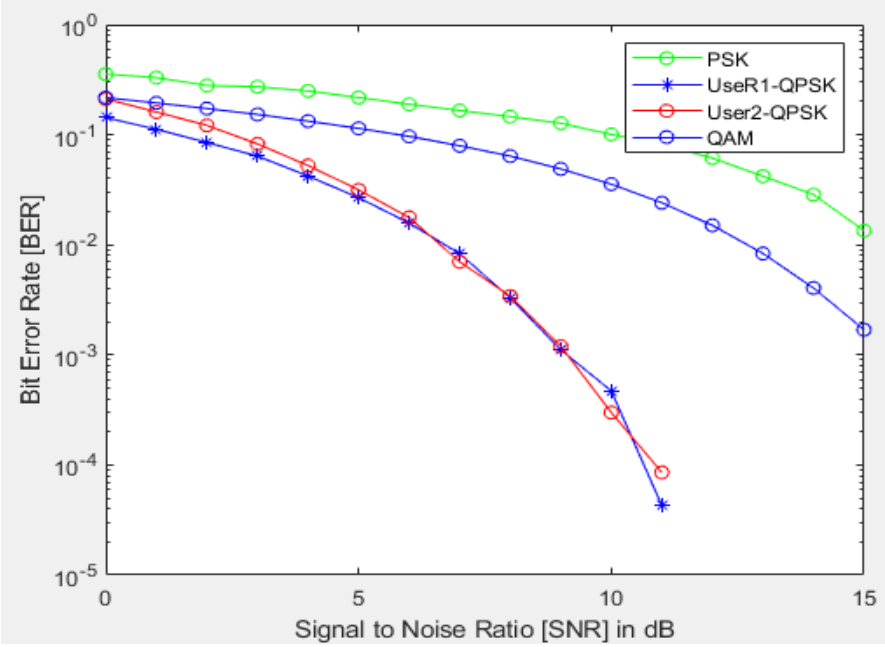

Figure 35: BER Simulation result of PSK, QPSK and QAM modulation

Figure 35 of the BER graph demonstrates that, of all transmission modulation techniques, QPSK modulation had the highest performance across all SNR levels, particularly at 10 dB we have obtain 10^{-4} while QAM and PSK modulation is at 10^{-2} and 10^{-1} respectively.

Similarly, the received signal bit error rate curve at 1.5m distance was displayed to demonstrate signal performance. Despite using PSK modulation, user 1 and user 2 achieved 0.4 Ber greater performance with QPSK modulation approaches.

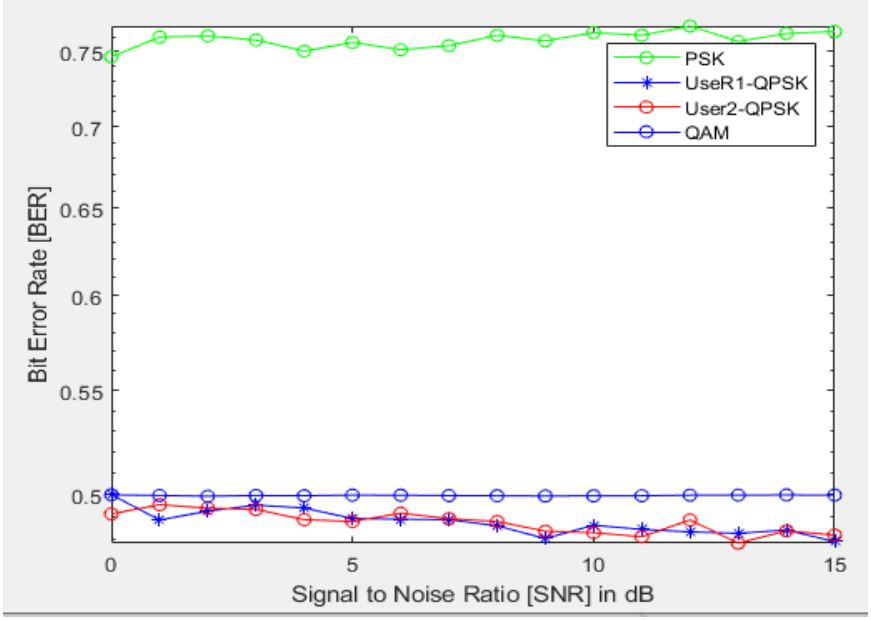

Figure 36: Implementation BER result of PSK, QPSK and QAM modulation

Chapter 6
Conclusion and Future Work

6.1 Conclusion

We presented a short-range Ultraviolet communication system using UV-A LED and NOMA methods in this study. This communication system has undergone both simulation and hardware testing.

We discussed the project's background in Chapter 1. It highlights the current research state of NOMA technologies and UV LED, as well as their research directions and obstacles, as well as their advantages and disadvantages. It also provides a synopsis of the related work.

We discussed UV light sources, their spectrum wavelengths, and UV LED detectors, which are instruments that measure the amount of ultraviolet light absorbed by the sample molecules, in Chapter 2. We also talked about how UV light can be used as a medium of communication in other domains.

The third chapter clearly addressed important topics such as OFDM, NOMA, and the SIC process. When NOMA-OFDM is utilized to transmit LED signals. Because the IFFT process in OFDM modulation necessitates the conjugated extension of the signal as well as the addition of a DC bias to the signal before it can be sent by LED. However, NOMA-OFDM offers a higher spectrum efficiency than other schemes. The NOMA-DCO-OFDM system and the SIC technique, which are critical for distinguishing between NOMA users, were then introduced. Implementing NOMA and OFDM together provides benefits, such as increasing channel utility, which is efficient

bandwidth usage, and minimizing noise impacting Ultraviolet signal by sending over a few of channels.

The main focus of Chapter 5 was the simulation of the NOMA-OFDM system for two users. In order to compare them, a variety of modulation approaches were applied. Change the power ratio between these two users to evaluate the BER performance of this system. The results show that modulation schemes like as BPSK, 4PSK, and 4QAM can function effectively in such a system, with QPSK standing out as having a very good BER. Previous research has used modulation methods such as BPSK, 4QAM, 4PSK, and so on. [41] We chose the QPSK modulation technique because it provides excellent overall performance in terms of bandwidth efficiency and bit error rate.

We have considered an only 2-user's scenario, but since its indoor experiment we can have good results. As the results shows by using the UV-A µLED, the bit error ratio of 4.30×10^{-4} is achieved. The achieved maximum distance between LEDs and APD Detector is 1.5 m. With higher power ratio, the BER is smaller. However, because of the distortion in devices and interference between 2-LEDs.

6.2 Challenges and Future Work

The NOMA-OFDM system configuration used in this work is not ideal, as indicated by the trial findings. When the output signals of these two Tx ports can transmit the identical signal with minimum distortion, the BER performance of this system will significantly improve. On the other hand, because it will be utilized in a room, a greater distance must exist between the transmitter and the receiver. As a result, more powerful LEDs with the potential to transmit brighter light are required. The NOMA-OFDM system can send optical signals over long distances and from various places.

Because this is an inside experiment, the distance between transmitter and receiver can be reduced but can potentially be greater than 1.5m. We examined Line of Sight (LOS) condition in this research, but we can transmit signal from multiple positions, different angles, and so on. We only explored a two-user scenario; however, a four-user or eight-user (n-user) scenario might be considered in the future. However, if the number of users increases, the NOMA-DCO-OFDM system may necessitate the application of power allocation and grouping technologies to differentiate between different users.

References

[1] X. Sun, B.S. Ooi, “HIGH DATA RATE OPTICAL WIRELESS COMMUNICATIONS BASED ON ULTRAVIOLET BAND”, October 2017.

[2] AK Majumdar, “Advanced Free Space Optics (FSO): A Systems Approach”, 2014.

[3] Mohammad Hamed Patmal, Jiang Liu, Shigeru Shimamoto, “Short-range high data rate WDM Ultraviolet-A LED-based communication link”, IEICE Communication Society Symposium Session BS-4-132019.

[4] M Uysal, C Capsoni, Z Ghassemlooy, A Boucouvalas, E Udvary. Optical wireless communications: an emerging technology. Springer, 2016.

[5] MP Lin, CJ Chen, LW Shan, MC Wu, Fabrication and characterization of 395 nm ultraviolet GaN light-emitting diodes, Solid-State Electronics, 2017.

[6] R. C. Kizilirmak, "Non-Orthogonal Multiple Access (NOMA) for 5G Networks", in Towards 5G Wireless Networks - A Physical Layer Perspective. London, United Kingdom: IntechOpen, 2016 [Online]. Available: https://www.intechopen.com/chapters/52822

[7] A. Benjebbour, K. Saito, A. Li, Y. Kishiyama and T. Nakamura, "Non-orthogonal multiple access (NOMA): Concept, performance evaluation and experimental trials," 2015 International Conference on Wireless Networks and Mobile Communications (WINCOM), 2015, pp. 1-6, doi: 10.1109/WINCOM.2015.7381343.

[8] D. N. Shubin, E. M. Lobov and V. O. Varlamov, "Overview of the NLOS Ultraviolet Communication Technology," 2020 Systems of Signal Synchronization, Generating and Processing in Telecommunications (SYNCHROINFO), 2020, pp. 1-6, doi: 10.1109/SYNCHROINFO49631.2020.9166129.

[9] Xiangyu He, Enyuan Xie, Mohamed Sufyan Islim, Ardimas Andi Purwita, Jonathan J. D. McKendry, Erdan Gu, Harald Haas, and Martin D. Dawson, "1 Gbps free-space deep-ultraviolet communications based on III-nitride micro-LEDs emitting at 262 nm," Photon. Res. 7, B41-B47 (2019)

[10] D. Kedar, and S. Arnon, “Subsea ultraviolet solar-blind broadband free-space optics communication,” Opt. Eng. 48(4), 046001 (2009).

[11] Y. Xing, M. Zhang, “Experimental Study of a 2x2 MIMO Scheme for ultraviolet communications”, IEEE, ICOCN, 978-1-5090-3491-8, Sept. 2016.

[12] Sun, X.; Zhang, Z.; Chaaban, A.; Ng, T. K.; Shen, C.; Chen, R.; Yan, J.; Sun, H.; Li, X.; Wang, J.; Li, J.; Alouini, M.-S.; Ooi, B. S. 71-Mbit/s ultraviolet-B LED communication link based on 8-QAM-OFDM modulation. Opt. Express 2017, 25, 23267– 23274, DOI: 10.1364/OE.25.023267.

[13]https://www.digikey.com/en/articles/ultraviolet-radiation-attributes-and-benefits

[14] http://solar-center.stanford.edu/about/uvlight.html

[15] https://dronebotworkshop.com/arduino-uv-index-meter/

[16] Uses for UV — Science Learning Hub

[17] Ultraviolet Light Disinfection - Bing images

[18] UV Light Curing 3D Printing - Bing images

[19https://sites.google.com/site/uvraysallyouneedtoknow/generalinformation

[20] https://www.intl-lighttech.com/applications/uvc-leds

[21] https://www.trojantechnologies.com/en/technologies/uv-lamps

[22]https://lab-training.com/characteristics-of-uv-vis-spectrophotometric-detectors/

[23]https://www.smacgigworld.com/blog/types-of-detectors-used-in-uv-vis-spectroscopy-system.php

[24]https://www.radiation-dosimetry.org/what-is-photomultiplier-tube-pmt-definition/

[25] Guo, Liang & Guo, Yanan & Wang, Junxi & Wei, Tongbo. (2021). Ultraviolet communication technique and its application. Journal of Semiconductors. 42. 081801. 10.1088/1674-4926/42/8/081801.

[26] Vasilyev, Gleb & Kuzichkin, Oleg & Surzhik, D.I. & Kharchuk, vetlana. (2020). Application of communication systems via the ultraviolet channel in FANET networks. MATEC Web of Conferences. 309. 01013. 10.1051/matecconf/202030901013.

[27]https://www.networkworld.com/article/3572372/military-looks-to-ultraviolet-networks-for-secure-battlefield communication.

[28] L Liao, Long Distance Non-Line-of-Sight Ultraviolet Communication Channel Analysis and Experimental Verification, UC Riverside, 2015.

[29] D. Tse and P. Vishwanathan, Multiuser Capacity and Opportunistic Communication, Fundamentals of Wireless Communication, Cambridge University Press, 2005.

[30] Tang, Tao, Yulong Mao, and Guangmin Hu. 2020. "A Fair Power Allocation Approach to OFDM-Based NOMA with Consideration of Clipping" Electronics 9, no.10:1743.https://doi.org/10.3390/electronics9101743.

[31] M., Ramesh, C., Shekar, N.C. (2021). Performance of Fading Channels in Non-orthogonal Multiple Access. In: Sengodan, T., Murugappan, M., Misra, S. (eds) Advances in Electrical and Computer Technologies. Lecture Notes in Electrical Engineering, vol 711. Springer, Singapore.

[32] R. C. Kizilirmak, "Non-Orthogonal Multiple Access (NOMA) for 5G Networks", in Towards 5G Wireless Networks - A Physical Layer Perspective. London, United Kingdom: IntechOpen, 2016 [Online]. Available: https://www.intechopen.com/chapters/52822.

[33] S. Kaur, N. Singh, G. Kaur and J. Singh, "Performance Comparison of BPSK, QPSK and 16-QAM Modulation Schemes in OFDM System using Reed-Solomon Codes," 2018 International Conference on Recent Innovations in Electrical, Electronics & Communication Engineering (ICRIEECE), 2018, pp. 530-533, doi: 10.1109/ICRIEECE44171.2018.9008983.

[34]https://rfmw.em.keysight.com/wireless/helpfiles/89600B/WebHelp/Subsystems/wlan-ofdm/Content/ofdm_basicprinciplesoverview.html.

[35] M. M. Madankar and P. S. Ashtankar, "Performance analysis of BPSK modulation scheme for different channel conditions," 2016 IEEE Students' Conference on Electrical, Electronics and Computer Science (SCEECS), 2016, pp. 1-5, doi: 10.1109/SCEECS.2016.7509290.

[36] https://en.wikipedia.org/wiki/Phase-shift_keying

[37] A. Sharma, S. Majumdar, A. Naugarhiya, B. Acharya, S. Majumder and S. Verma, "VERILOG based simulation of ASK, FSK, PSK, QPSK digital modulation techniques," 2017 International Conference on I-SMAC (IoT in Social, Mobile, Analytics and Cloud) (I-SMAC), 2017, pp. 403-408, doi: 10.1109/I-SMAC.2017.8058380.

[38] A. Svensson, "An Introduction to Adaptive QAM Modulation Schemes for Known and Predicted Channels," in Proceedings of the IEEE, vol. 95, no. 12, pp. 2322-2336, Dec. 2007, doi: 10.1109/JPROC.2007.904442.

[39] N. L. M. Hweesa, A. R. Zerek and A. M. Daeri, "Investigation the Performance Effect of Adjacent and Co-Channel Interferences on AWGN and Rayleigh Channels Using16-QAM Modulation," 2020 17th International Multi-Conference on Systems, Signals & Devices (SSD), 2020, pp. 1052-1057, doi: 10.1109/SSD49366.2020.9364192.

[40]https://www.ledsupply.com/content/leds-semiled-uvdocumentation.pdf

[41] Ziyao Zhang, Yuyu Ying, Jiang Liu and Shigeru Shimamoto, "Experimental Studies of NOMA-VLC scheme," in IEICE conference, Higashi Hiroshima city, March 17-20, 2020.

[42] Y Muramoto, M Kimura, S Nouda, Development and future of ultraviolet lightemitting diodes: UV-LED will replace the UV lamp, Semiconductor Science and Technology, 2014.